

An advanced meshless approach for the high-dimensional multi-term time-space-fractional PDEs on general domains

X. G. Zhu · Y. F. Nie · J. G. Wang · Z. B. Yuan

Received: date / Accepted: date

Abstract In this article, an advanced differential quadrature (DQ) approach is proposed for the high-dimensional multi-term time-space-fractional partial differential equations (TSFPDEs) on general domains. Firstly, a family of high-order difference schemes is introduced to discretize the time-fractional derivative and a semi-discrete scheme for the considered problems is presented. We strictly prove its unconditional stability and error estimate in time. Further, we derive a class of DQ formulas to evaluate the fractional derivatives, which employs radial basis functions (RBFs) as test functions. Using these DQ formulas in spatial discretization, a fully discrete DQ scheme is then proposed. Our approach provides a flexible and high accurate alternative to solve the high-dimensional multi-term TSFPDEs on general domains and its actual performance is illustrated by contrast to the other methods available in the open literature. The numerical results finally confirm the theoretical analysis as well as its capability and advantages.

Keywords Radial basis functions · Differential quadrature · high-order difference operator · Multi-term time-space fractional partial differential equation

1 Introduction

The fractional partial differential equations (PDEs) are the results of mathematical modelling based on the frac-

X. G. Zhu
School of Science, Shaoyang University, Shaoyang, Hunan 422000, P.R. China
E-mail: zhuxg590@yeah.net

Y. F. Nie · J. G. Wang · Z. B. Yuan
Department of Applied Mathematics, Northwestern Polytechnical University, Xi'an, Shaanxi 710129, P. R. China
E-mail: yfnie@nwpu.edu.cn

tional calculus, which provides a new powerful tool to study some complex systems associated with temporal memory or long-range space interaction in mathematical physics or even the whole scientific research. Nevertheless, there raises a challenge to solve these type of equations and few of fractional PDEs can be solved by analytic techniques. As a result, numerical methods are clearly priority for development. The fractional PDEs can be divided into three categories: the time-fractional PDEs, the space-fractional PDEs, and a mixture of both. Up to present, the numerical algorithms for the time-fractional PDEs are on the way to maturity after recent years' development [20, 21, 23, 26, 33, 40, 46, 49], while these for the high-dimensional space-fractional or time-space-fractional PDEs have to be further developed and improved. Regardless of the difficulties in constructing numerical algorithms for the space-fractional PDEs, many methods have been invented to solve them, which covers the mainstream of today's numerical methods, such as finite difference (FD) methods [6, 22, 32, 42], spectral methods [4, 47], finite element (FE) methods [12, 15, 48, 50], and finite volume methods [18, 41]. Liu et al. considered a space-fractional FitzHugh-Nagumo monodomain model by an implicit semi-alternative direction FD scheme on approximate irregular domains [28]. Qiu et al. developed a nodal discontinuous Galerkin method for the two-dimensional space-fractional diffusion equations [38]. Yang et al. studied a FE method for the two-dimensional nonlinear space-fractional diffusion equations on convex domains [44]. Bhrawy and Zaky developed a Jacobi spectral tau method for the multi-term TSFPDEs [5]. In [11], an efficient numerical algorithm based on FD and FE methods was addressed for the two-dimensional multi-term time-space-fractional Bloch-Torrey equations. Qin et al. gave a fully discrete FE scheme for the multi-term time and

space fractional Bloch-Torrey equation based on bilinear rectangular finite elements [37]. Fan et al. proposed a fully discrete FE scheme with unstructured meshes for the two-dimensional multi-term time-space fractional diffusion-wave equations on convex domains [16].

Although the study of numerical methods for the fractional PDEs is an active area of research, few works have been reported for the high-dimensional multi-term TSFPDEs on general domains. Actually, this topic is full of challenges because of the non-locality and weakly singular integral kernel of fractional derivatives, which is the biggest difficulty in the design of their numerical algorithms. This situation motivates us to seek another efficient numerical methods to solve these equations. Meshless methods have the ability to construct functional approximation entirely from information at a set of scattered nodes or particles, and thereby can reduce the computational cost in practise. They serve as promising alternatives in dealing with the structure destruction, high-dimensional crack propagation, and large deformation problems without the expensive mesh generation. In the past two decades, meshless methods have achieved significant advances and many meshless methods have been developed, such as diffuse element method [34], reproducing kernel particle (RKP) method [19], hp-cloud method, element-free Galerkin method [3], meshless local Petrov-Galerkin method [1], boundary element-free method, Kansa's methods [17, 24], point interpolation (PI) method [29], and so forth. Meshless methods offer more advantages over the mesh-dependent methods in treating the space-fractional PDEs but seldom works have bee reported in this field, let alone the multi-term TSFPDEs. Liu et al. addressed a meshless PI technique in strong form for the space-fractional diffusion equation [31]. Cheng et al. proposed an improved moving least-squares collocation scheme for the two-dimensional two-sided space-fractional wave equation [10]. In [45], the meshless PI method based on weak form was further developed for the space fractional advection-dispersion equations.

The basic principle of DQ method was suggested by Bellman and Casti in 1971 [2], and due to the rapid development of computer simulation, this method has recently aroused extensive concern because it is rather simple to perform and can use a few nodes to achieve high accuracy. During recent decades, many scholars applied different basis functions to develop different DQ methods, such as polynomial DQ method [14], Hermite polynomial DQ [9], splines-based DQ method, orthogonal polynomial DQ method [39], and RBFs-based DQ method [43]. At present, a certain progress was made in the new development of DQ methods, which mostly makes sense to mechanical analysis. Some are

committed to the researches of the method itself and some are committed to its new areas of application in structural engineering. In fractional cases, Pang et al. extended the classical polynomial DQ method to the steady-state space-fractional advection-diffusion equations [36], where the Lagrange interpolation basis functions are used as test functions to determine weighted coefficients. In [51], we proposed an effective DQ method for the two-dimensional space-fractional diffusion equations by using RBFs as test functions. Liu et al. applied the RBFs-based DQ method for the numerical simulation of two-dimensional variable-order time-fractional advection-diffusion equation [30].

In this work, we will showcase an efficient RBFs-based DQ method for the high-dimensional multi-term TSFPDEs on general domains:

(i) two-dimensional multi-term TSFPDE:

$$\left\{ \begin{array}{l} P_{\theta_1, \theta_2, \dots, \theta_s} ({}_0^C \mathcal{D}_t) u(x, y, t) - \varepsilon_\alpha^+(x, y) \frac{\partial_+^\alpha u(x, y, t)}{\partial x_+^\alpha} \\ - \varepsilon_\alpha^-(x, y) \frac{\partial_-^\alpha u(x, y, t)}{\partial x_-^\alpha} - \varepsilon_\beta^+(x, y) \frac{\partial_+^\beta u(x, y, t)}{\partial y_+^\beta} \\ - \varepsilon_\beta^-(x, y) \frac{\partial_-^\beta u(x, y, t)}{\partial y_-^\beta} \\ = f(x, y, t), \quad (x, y; t) \in \Omega \times (0, T], \\ u(x, y, 0) = u_0(x, y), \quad (x, y) \in \Omega, \\ u(x, y, t) = g(x, y, t), \quad (x, y; t) \in \partial\Omega \times (0, T], \end{array} \right. \quad (1)$$

where $0 < \theta_1, \theta_2, \dots, \theta_s \leq 1$, $s \in \mathbb{Z}^+$, $1 < \alpha, \beta \leq 2$, $\Omega \subset \mathbb{R}^2$ with $\partial\Omega$ being its boundary, $\varepsilon_\varsigma^\pm(x, y)$ are the diffusion coefficients with $\varsigma = \alpha, \beta$.

(ii) three-dimensional multi-term TSFPDE:

$$\left\{ \begin{array}{l} P_{\theta_1, \theta_2, \dots, \theta_s} ({}_0^C \mathcal{D}_t) u(x, y, z, t) - \varepsilon_\alpha^+(x, y, z) \frac{\partial_+^\alpha u(x, y, z, t)}{\partial x_+^\alpha} \\ - \varepsilon_\alpha^-(x, y, z) \frac{\partial_-^\alpha u(x, y, z, t)}{\partial x_-^\alpha} - \varepsilon_\beta^+(x, y, z) \frac{\partial_+^\beta u(x, y, z, t)}{\partial y_+^\beta} \\ - \varepsilon_\beta^-(x, y, z) \frac{\partial_-^\beta u(x, y, z, t)}{\partial y_-^\beta} - \varepsilon_\gamma^+(x, y, z) \frac{\partial_+^\gamma u(x, y, z, t)}{\partial z_+^\gamma} \\ - \varepsilon_\gamma^-(x, y, z) \frac{\partial_-^\gamma u(x, y, z, t)}{\partial z_-^\gamma} \\ = f(x, y, z, t), \quad (x, y, z; t) \in \Omega \times (0, T], \\ u(x, y, z, 0) = u_0(x, y, z), \quad (x, y, z) \in \Omega, \\ u(x, y, z, t) = g(x, y, z, t), \quad (x, y, z; t) \in \partial\Omega \times (0, T], \end{array} \right. \quad (2)$$

where $0 < \theta_1, \theta_2, \dots, \theta_s \leq 1$, $s \in \mathbb{Z}^+$, $1 < \alpha, \beta, \gamma \leq 2$, $\Omega \subset \mathbb{R}^3$ with $\partial\Omega$ being its boundary, $\varepsilon_\varsigma^\pm(x, y, z)$ are the diffusion coefficients with $\varsigma = \alpha, \beta, \gamma$.

Assuming $C_1 : x = x_L(y, z)$, $C_2 : x = x_R(y, z)$ are the forward and backward boundaries, $C_3 : y =$

$y_L(x, z), C_4 : y = y_R(x, z)$ are the left and right boundaries, and $C_5 : z = z_L(x, y), C_6 : z = z_R(x, y)$ are the lower and upper boundaries of $\Omega \subset \mathbb{R}^3$, in which

$$x_L(y, z) = \min\{x : (x, \eta, \zeta), \eta = y, \zeta = z\},$$

$$x_R(y, z) = \max\{x : (x, \eta, \zeta), \eta = y, \zeta = z\},$$

$$y_L(x, z) = \min\{y : (\eta, y, \zeta), \eta = x, \zeta = z\},$$

$$y_R(x, z) = \max\{y : (\eta, y, \zeta), \eta = x, \zeta = z\},$$

$$z_L(x, y) = \min\{z : (\eta, \zeta, z), \eta = x, \zeta = y\},$$

$$z_R(x, y) = \max\{z : (\eta, \zeta, z), \eta = x, \zeta = y\},$$

the space-fractional derivatives are defined as follows:

$$\begin{aligned} \frac{\partial^\alpha_+ u(x, y, z, t)}{\partial x_+^\alpha} &= \frac{1}{\Gamma(2-\alpha)} \int_{x_L(y, z)}^x \frac{\partial^2 u(\xi, y, z, t)}{\partial \xi^2} \frac{d\xi}{(x-\xi)^{\alpha-1}}, \\ \frac{\partial^\alpha_- u(x, y, z, t)}{\partial x_-^\alpha} &= \frac{1}{\Gamma(2-\alpha)} \int_x^{x_R(y, z)} \frac{\partial^2 u(\xi, y, z, t)}{\partial \xi^2} \frac{d\xi}{(\xi-x)^{\alpha-1}}, \\ \frac{\partial^\beta_+ u(x, y, z, t)}{\partial y_+^\beta} &= \frac{1}{\Gamma(2-\beta)} \int_{y_L(x, z)}^y \frac{\partial^2 u(x, \xi, z, t)}{\partial \xi^2} \frac{d\xi}{(y-\xi)^{\beta-1}}, \\ \frac{\partial^\beta_- u(x, y, z, t)}{\partial y_-^\beta} &= \frac{1}{\Gamma(2-\beta)} \int_y^{y_R(x, z)} \frac{\partial^2 u(x, \xi, z, t)}{\partial \xi^2} \frac{d\xi}{(\xi-y)^{\beta-1}}, \\ \frac{\partial^\gamma_+ u(x, y, z, t)}{\partial z_+^\gamma} &= \frac{1}{\Gamma(2-\gamma)} \int_{z_L(x, y)}^z \frac{\partial^2 u(x, y, \xi, t)}{\partial \xi^2} \frac{d\xi}{(z-\xi)^{\gamma-1}}, \\ \frac{\partial^\gamma_- u(x, y, z, t)}{\partial z_-^\gamma} &= \frac{1}{\Gamma(2-\gamma)} \int_z^{z_R(x, y)} \frac{\partial^2 u(x, y, \xi, t)}{\partial \xi^2} \frac{d\xi}{(\xi-z)^{\gamma-1}}, \end{aligned}$$

with the Gamma function $\Gamma(\cdot)$. $P_{\theta_1, \theta_2, \dots, \theta_s}({}_0^C \mathcal{D}_t)$ denotes the multi-term fractional derivative operator:

$$\begin{aligned} P_{\theta_1, \theta_2, \dots, \theta_s}({}_0^C \mathcal{D}_t) u(x, y, z, t) &= \sum_{r=1}^s a_r {}_0^C D_t^{\theta_r} u(x, y, z, t) \\ &= a_1 {}_0^C D_t^{\theta_1} u(x, y, z, t) + a_2 {}_0^C D_t^{\theta_2} u(x, y, z, t) \\ &\quad + \dots + a_s {}_0^C D_t^{\theta_s} u(x, y, z, t), \end{aligned} \quad (3)$$

where

$${}_0^C D_t^{\theta_r} u(x, y, z, t) = \begin{cases} \frac{\partial u(x, y, z, t)}{\partial t}, & \theta_r = 1, \\ \frac{1}{\Gamma(1-\theta_r)} \int_0^t \frac{\partial u(x, y, z, \xi)}{\partial \xi} \frac{d\xi}{(t-\xi)^{\theta_r}}, & 0 < \theta_r < 1, \end{cases}$$

where $a_1 \in \mathbb{R}^+$ and $a_r \geq 0$, $r = 2, 3, \dots, s$.

The layout is as follows. In Section 2, some preliminaries on the fractional calculus and RBFs are introduced. In Section 3, a family of high-order schemes of the time-fractional derivative is presented and a semi-discrete scheme is obtained. In Section 4, the unconditional stability and convergence are discussed. In Section 5, the DQ formulas for fractional derivatives are proposed based on RBFs, and with these RBFs-based DQ formulas, we further construct a fully discrete DQ

scheme for the multi-term TSFPDEs on general domains. In Section 6, some illustrative examples are carried out to confirm the validity and convergence. A concluding remark is given in Section 7.

2 Preliminaries

We recall some basic preliminaries on the fractional calculus and RBFs required for further discussions. Letting $\Omega \subset \mathbb{R}^d$, $d = 2, 3$, we define

$$(u, v) = \int_{\Omega} u v d\Omega, \quad \|u\|_{0, \Omega} = \sqrt{(u, u)}.$$

2.1 Fractional calculus

Definition 1 The left and right Riemann-Liouville fractional integrals of order α are defined by

$$\begin{aligned} {}_a J_x^\alpha u(x) &= \frac{1}{\Gamma(\alpha)} \int_a^x \frac{u(\xi) d\xi}{(x-\xi)^{1-\alpha}}, \quad x > a, \\ {}_x J_b^\alpha u(x) &= \frac{1}{\Gamma(\alpha)} \int_x^b \frac{u(\xi) d\xi}{(\xi-x)^{1-\alpha}}, \quad x < b, \end{aligned}$$

and if $\alpha = 0$, ${}_a J_x^\alpha u(x) = u(x)$ and ${}_x J_b^\alpha u(x) = u(x)$.

Definition 2 The left and right Riemann-Liouville fractional derivatives of order α are defined by

$$\begin{aligned} {}^{RL} D_x^\alpha u(x) &= \left(\frac{d}{dx} \right)^m {}_a J_x^{m-\alpha} u(x) \\ &= \frac{1}{\Gamma(m-\alpha)} \frac{d^m}{dx^m} \int_a^x \frac{u(\xi) d\xi}{(x-\xi)^{\alpha-m+1}}, \quad x > a, \\ {}^{RL} D_b^\alpha u(x) &= (-1)^m \left(\frac{d}{dx} \right)^m {}_x J_b^{m-\alpha} u(x) \\ &= \frac{(-1)^m}{\Gamma(m-\alpha)} \frac{d^m}{dx^m} \int_x^b \frac{u(\xi) d\xi}{(\xi-x)^{\alpha-m+1}}, \quad x < b, \end{aligned}$$

where $m-1 < \alpha < m$, $m \in \mathbb{Z}^+$, and if $\alpha = m$, ${}_a^{RL} D_x^\alpha u(x) = u^{(m)}(x)$ and ${}_x^{RL} D_b^\alpha u(x) = (-1)^m u^{(m)}(x)$.

Definition 3 The left and right Caputo fractional derivatives of order α are defined by

$$\begin{aligned} {}_a^C D_x^\alpha u(x) &= {}_a J_x^{m-\alpha} u^{(m)}(x) \\ &= \frac{1}{\Gamma(m-\alpha)} \int_a^x \frac{u^{(m)}(\xi) d\xi}{(\xi-x)^{\alpha-m+1}}, \quad x > a, \\ {}_x^C D_b^\alpha u(x) &= (-1)^m {}_x J_b^{m-\alpha} u^{(m)}(x) \\ &= \frac{(-1)^m}{\Gamma(m-\alpha)} \int_x^b \frac{u^{(m)}(\xi) d\xi}{(\xi-x)^{\alpha-m+1}}, \quad x < b, \end{aligned}$$

where $m-1 < \alpha < m$, $m \in \mathbb{Z}^+$, and if $\alpha = m$, ${}_a^C D_x^\alpha u(x) = u^{(m)}(x)$ and ${}_x^C D_b^\alpha u(x) = (-1)^m u^{(m)}(x)$.

Lemma 1 [15] For $\alpha \in \mathbb{R}^+$, the left and right Riemann-Liouville fractional derivatives have property

$$({}_a^{RL}D_x^\alpha u, {}_x^{RL}D_b^\alpha v) = \cos(\alpha\pi) \|{}_a^{RL}D_x^\alpha u\|_{0,\Omega}^2.$$

Lemma 2 [15] For $0 < \alpha < 1$, there exist

$$({}_a^{RL}D_x^{2\alpha} u, v) = ({}_a^{RL}D_x^\alpha u, {}_x^{RL}D_b^\alpha v),$$

$$({}_x^{RL}D_b^{2\alpha} u, v) = ({}_x^{RL}D_b^\alpha u, {}_a^{RL}D_x^\alpha v).$$

The Caputo and Riemann-Liouville fractional derivatives are converted to one another by the relation

$${}_a^C D_x^\alpha u(x) = {}_a^{RL} D_x^\alpha u(x) - \sum_{l=0}^{m-1} \frac{u^{(l)}(a)}{\Gamma(l+1-\alpha)} (x-a)^{l-\alpha},$$

$${}_x^C D_b^\alpha u(x) = {}_x^{RL} D_b^\alpha f(x) - \sum_{l=0}^{m-1} \frac{u^{(l)}(b)}{\Gamma(l+1-\alpha)} (b-x)^{l-\alpha}.$$

In addition, we have the properties:

$${}_a^C D_x^\alpha C = 0, \quad (4)$$

$${}_a J_x^{\alpha_1} {}_a J_x^{\alpha_2} u(x) = {}_a J_x^{\alpha_2} {}_a J_x^{\alpha_1} u(x) = {}_a J_x^{\alpha_1 + \alpha_2} u(x), \quad (5)$$

$$\begin{aligned} {}_a^C D_x^\alpha (x-a)^\beta &= {}_a^{RL} D_x^\alpha (x-a)^\beta \\ &= \frac{\Gamma(1+\beta)}{\Gamma(1+\beta-\alpha)} (x-a)^{\beta-\alpha}, \end{aligned} \quad (6)$$

where C is a constant and $\beta > [\alpha] + 1$ with $[x]$ being the ceiling function, which outputs the smallest integer greater than or equal to x . Another point need to be noticed is that these properties are also true for the right-side fractional calculus. For more details, we refer the readers to [25] for deeper insights.

2.2 Radial basis functions

Letting $\mathbf{x} = (x_1, x_2, \dots, x_d)$, $\{\mathbf{x}_i\}_{i=0}^M \in \Omega \subset \mathbb{R}^d$, the approximation of $u(\mathbf{x})$ can be written as a weighted sum of RBFs in the form:

$$u(\mathbf{x}) \approx \sum_{i=0}^M \lambda_i \varphi(r_i) + \sum_{q=1}^Q \mu_q p_q(\mathbf{x}), \quad \mathbf{x} \in \Omega, \quad (7)$$

where

$$Q = \binom{d}{n+d-1}, \quad d = 1, 2, 3,$$

and $\{\lambda_i\}_{i=0}^M$, $\{\mu_q\}_{q=1}^Q$ are unknown weights, $\{p_q(\mathbf{x})\}_{q=1}^Q$ are the basis functions of the polynomial space of degree at most $n-1$, and $\{\varphi(r_i)\}_{i=0}^M$ are RBFs with $r_i = \|\mathbf{x}_i - \mathbf{x}\|$. To ensure that the interpolant properly behave at infinity, the above equations are augmented by

$$\sum_{i=0}^M \lambda_i p_q(\mathbf{x}_i) = 0, \quad q = 1, 2, \dots, Q. \quad (8)$$

Put Eqs. (7)-(8) in the below form

$$\begin{bmatrix} \mathbf{A} & \mathbf{B}^T \\ \mathbf{B} & \mathbf{0} \end{bmatrix} \begin{pmatrix} \boldsymbol{\lambda} \\ \boldsymbol{\mu} \end{pmatrix} = \begin{pmatrix} \mathbf{u} \\ \mathbf{0} \end{pmatrix}, \quad (9)$$

where the matrix elements for $[\mathbf{A}]$ are $\varphi(r_{ij})$ and for $[\mathbf{B}]$ are $p_j(\mathbf{x}_i)$ with $r_{ij} = \|\mathbf{x}_j - \mathbf{x}_i\|$. $\boldsymbol{\lambda}$, $\boldsymbol{\mu}$, and \mathbf{u} are column vectors and the vector elements for them are λ_i , μ_i , and $u(\mathbf{x}_i)$, respectively.

Definition 4 A function is completely monotonic if and only if $(-1)^\ell f^{(\ell)}(r) \geq 0$ for $\ell = 0, 1, 2, \dots$, and $r \geq 0$.

Theorem 1 [8] Let an univariate function $\psi(r) \in C^\infty[0, +\infty)$ be such that ψ is completely monotonic, but not a constant. Suppose further that $\psi(0) \geq 0$. Then the interpolation matrix $[\mathbf{A}]$ of the basis function $\varphi(r) = \psi(r^2)$ is positive definite.

The Eq. (9) is solved to obtain $\{\lambda_i\}_{i=0}^M$, $\{\mu_q\}_{q=1}^Q$. If $r = \|\cdot\|$, we give the commonly used RBFs in Table 1, where c is the shape parameter. According to Theorem 1, except Multiquadratics and Polyharmonic Splines, the interpolation matrices $[\mathbf{A}]$ of the other three RBFs have all positive eigenvalues, i.e., $[\mathbf{A}]$ is invertible and the polynomial term in Eq. (7) can be removed. Multiquadratics do not fulfill the above theorem and actually the eigenvalues remain the ones that are negative. To keep the well-posedness of the resulting algebraic system, the polynomial term is thus necessary, i.e., $Q \geq 1$.

3 The temporal discretization

In this section, we introduce a family of high-order difference schemes to discretize the fractional derivative in time. Define a grid $t_n = n\tau$, $n = 0, 1, \dots, N$, $T = \tau N$, $N \in \mathbb{Z}^+$, on the time interval $[0, T]$, and denote the Lubich's difference operator by

$$\mathcal{L}_q^\theta u(\mathbf{x}, t_n) = \frac{1}{\tau^\theta} \sum_{k=0}^n \omega_k^{q,\theta} u(\mathbf{x}, t_{n-k}),$$

which is always used to discretize the Riemann-Liouville of order θ [7], where $m-1 < \theta < m$, $m \in \mathbb{Z}^+$, and $q = 1, 2, 3, 4, 5$. By virtue of the relation of both fractional derivatives, there exists

$${}_0^C D_t^\theta u(\mathbf{x}, t) = {}_0^{RL} D_t^\theta u(\mathbf{x}, t) - \sum_{l=0}^{m-1} \frac{u_t^{(l)}(\mathbf{x}, 0) t^{l-\theta}}{\Gamma(l+1-\theta)}. \quad (10)$$

Using the property (6) and applying the operator \mathcal{L}_q^θ to discretize the Riemann-Liouville derivatives in

Table 1 Some commonly used RBFs.

Name	RBF
Multiquadric (MQ)	$\varphi(r) = (r^2 + c^2)^{1/2}, c > 0$
Inverse Multiquadric (IMQ)	$\varphi(r) = 1/(r^2 + c^2)^{1/2}, c > 0$
Inverse Quadratic (IQ)	$\varphi(r) = 1/(r^2 + c^2), c > 0$
Gaussian (GA)	$\varphi(r) = e^{-r^2/c^2}, c > 0$
Polyharmonic Spline (PS)	$\varphi(r) = (-1)^{s+1} r^{2s} \ln r, s \in \mathbb{Z}^+$

Eq. (10) lead to

$$\begin{aligned} {}_0^C D_t^\theta u(\mathbf{x}, t_n) &\approx \frac{1}{\tau^\theta} \sum_{k=0}^n \omega_k^{q,\theta} u(\mathbf{x}, t_{n-k}) \\ &\quad - \frac{1}{\tau^\theta} \sum_{l=0}^{m-1} \sum_{k=0}^n \frac{\omega_k^{q,\theta} u_t^{(l)}(\mathbf{x}, 0) t_{n-k}^l}{l!}, \end{aligned} \quad (11)$$

where $\{\omega_k^{q,\theta}\}_{k=0}^n$ are the discrete coefficients. For example, when $q = 1$, we have $\omega_k^{1,\theta} = \frac{\Gamma(k-\theta)}{\Gamma(-\theta)\Gamma(k+1)}$, $k = 0, 1, 2, \dots$, and denote $\omega_k^{1,\theta}$ by ω_k^θ hereafter.

Lemma 3 The coefficients ω_k^θ satisfy the properties

$$\begin{aligned} (i) \quad &\omega_0^\theta = 1, \quad \omega_k^\theta < 0, \quad \sum_{k=0}^\infty \omega_k^\theta = 0, \quad \sum_{k=0}^{n-1} \omega_k^\theta > 0, \quad \forall k = 1, 2, \dots, \\ (ii) \quad &\omega_0^\theta = 1, \quad \omega_k^\theta = \left(1 - \frac{\theta+1}{k}\right) \omega_{k-1}^\theta, \quad \forall k = 1, 2, \dots \end{aligned}$$

Moreover, by virtue of $\sum_{k=1}^\infty \omega_k^\theta = -1$ and $\omega_k^\theta < 0$, $k \neq 0$, we can derive $-1 < \omega_k^\theta < 0$ for $k = 1, 2, 3, \dots$

Lemma 4 [7] Assume that $u(\mathbf{x}, t)$, ${}_{-\infty}^{RL} D_t^{\theta+q} u(\mathbf{x}, t)$ and their Fourier transforms belong to $L^1(\mathbb{R})$ with regard to t , then the Lubich's difference operators satisfy

$${}_0^{RL} D_t^\theta u(\mathbf{x}, t_n) = \mathcal{L}_q^\theta u(\mathbf{x}, t_n) + \mathcal{O}(\tau^q). \quad (12)$$

Theorem 2 Assume that $u(\mathbf{x}, t)$ with $\theta > 0$ is smooth enough with regard to t , then we have

$${}_0^C D_t^\theta u(\mathbf{x}, t_n) = \mathcal{A}_q^\theta u(\mathbf{x}, t_n) + \mathcal{O}(\tau^q), \quad (13)$$

where

$$\begin{aligned} \mathcal{A}_q^\theta u(\mathbf{x}, t_n) &= \frac{1}{\tau^\theta} \sum_{k=0}^n \omega_k^{q,\theta} u(\mathbf{x}, t_{n-k}) \\ &\quad - \frac{1}{\tau^\theta} \sum_{l=0}^{m-1} \sum_{k=0}^n \frac{\omega_k^{q,\theta} u_t^{(l)}(\mathbf{x}, 0) t_{n-k}^l}{l!}. \end{aligned}$$

The proof is trivial by following Lemma 4. Letting $0 < \theta_1, \theta_2, \dots, \theta_s \leq 1$ and applying the operators $\mathcal{A}_q^{\theta_r}$

to the multi-term fractional derivative operator, we finally have

$$\begin{aligned} &P_{\theta_1, \theta_2, \dots, \theta_s} ({}_0^C \mathcal{D}_t) u(\mathbf{x}, t_n) \\ &= a_1 {}_0^C D_t^{\theta_1} u(\mathbf{x}, t_n) + a_2 {}_0^C D_t^{\theta_2} u(\mathbf{x}, t_n) \\ &\quad + \dots + a_s {}_0^C D_t^{\theta_s} u(\mathbf{x}, t_n) \\ &= a_1 \mathcal{A}_q^{\theta_1} u(\mathbf{x}, t_n) + a_2 \mathcal{A}_q^{\theta_2} u(\mathbf{x}, t_n) \\ &\quad + \dots + a_s \mathcal{A}_q^{\theta_s} u(\mathbf{x}, t_n) + \mathcal{O}(\tau^q) \\ &= \sum_{r=1}^s a_r \mathcal{A}_q^{\theta_r} u(\mathbf{x}, t_n) + \mathcal{O}(\tau^q) \\ &= \sum_{r=1}^s \frac{a_r}{\tau^{\theta_r}} \sum_{k=0}^{n-1} \omega_k^{q,\theta_r} u(\mathbf{x}, t_{n-k}) \\ &\quad - \sum_{r=1}^s \frac{a_r}{\tau^{\theta_r}} \sum_{k=0}^{n-1} \omega_k^{q,\theta_r} u(\mathbf{x}, 0) + \mathcal{O}(\tau^q). \end{aligned} \quad (14)$$

We derive the semi-discretization in time for Eqs. (1)-(2) and for simplicity, letting $\mathbf{x} = (x_1, x_2, \dots, x_d)$, $\Omega \subset \mathbb{R}^d$, we put Eqs. (1)-(2) in a unified form:

$$\begin{cases} P_{\theta_1, \theta_2, \dots, \theta_s} ({}_0^C \mathcal{D}_t) u(\mathbf{x}, t) - \sum_{l=1}^d \varepsilon_{\alpha_l}^+(\mathbf{x}) \frac{\partial_{+}^{\alpha_l} u(\mathbf{x}, t)}{\partial x_{l,+}^{\alpha_l}} \\ \quad - \sum_{l=1}^d \varepsilon_{\alpha_l}^-(\mathbf{x}) \frac{\partial_{-}^{\alpha_l} u(\mathbf{x}, t)}{\partial x_{l,-}^{\alpha_l}} = f(\mathbf{x}, t), \quad (\mathbf{x}; t) \in \Omega \times (0, T], \\ u(\mathbf{x}, 0) = u_0(\mathbf{x}), \quad \mathbf{x} \in \Omega, \\ u(\mathbf{x}, t) = g(\mathbf{x}, t), \quad (\mathbf{x}; t) \in \partial\Omega \times (0, T], \end{cases}$$

where $0 < \theta_1, \theta_2, \dots, \theta_s \leq 1$, $1 < \alpha_l \leq 2$ and $l = 1, 2, \dots, d$.

Using the operator \mathcal{A}_q^θ to discretize $P_{\theta_1, \theta_2, \dots, \theta_s} ({}_0^C \mathcal{D}_t)$ arrives at

$$\begin{aligned} &\sum_{r=1}^s a_r \mathcal{A}_q^{\theta_r} u(\mathbf{x}, t_n) - \sum_{l=1}^d \varepsilon_{\alpha_l}^+(\mathbf{x}) \frac{\partial_{+}^{\alpha_l} u(\mathbf{x}, t_n)}{\partial x_{l,+}^{\alpha_l}} \\ &\quad - \sum_{l=1}^d \varepsilon_{\alpha_l}^-(\mathbf{x}) \frac{\partial_{-}^{\alpha_l} u(\mathbf{x}, t_n)}{\partial x_{l,-}^{\alpha_l}} = f(\mathbf{x}, t_n) + \mathcal{O}(\tau^q), \end{aligned} \quad (15)$$

Omitting the truncation error $\mathcal{O}(\tau^q)$, we obtain the following semi-discrete scheme:

$$\begin{aligned} & \sum_{r=1}^s \frac{a_r \omega_0^{q, \theta_r}}{\tau^{\theta_r}} U^n(\mathbf{x}) - \sum_{l=1}^d \varepsilon_{\alpha_l}^+(\mathbf{x}) \frac{\partial_+^{\alpha_l} U^n(\mathbf{x})}{\partial x_{l,+}^{\alpha_l}} \\ & - \sum_{l=1}^d \varepsilon_{\alpha_l}^-(\mathbf{x}) \frac{\partial_-^{\alpha_l} U^n(\mathbf{x})}{\partial x_{l,-}^{\alpha_l}} = f(\mathbf{x}, t_n) \\ & - \sum_{r=1}^s \frac{a_r}{\tau^{\theta_r}} \sum_{k=1}^{n-1} \omega_k^{\theta_r} U^{n-k}(\mathbf{x}) \\ & + \sum_{r=1}^s \frac{a_r}{\tau^{\theta_r}} \sum_{k=0}^{n-1} \omega_k^{\theta_r} U^0(\mathbf{x}), \quad n = 1, 2, \dots, N. \end{aligned} \quad (16)$$

4 Stability and convergent analysis

In this section, we attempt to strictly prove the stability and error estimate of the semi-discrete scheme (16). To this end, we assume $\varepsilon_{\alpha_l}^+(\mathbf{x}), \varepsilon_{\alpha_l}^-(\mathbf{x})$ are all constants $\varepsilon_{\alpha_l}^+, \varepsilon_{\alpha_l}^-$ and mainly focus on the case of $q = 1$. By Lemma 1, let us define the energy norm

$$\begin{aligned} |u|_{\alpha_l, \Omega} &= \left\{ \sum_{l=1}^d \varepsilon_{\alpha_l}^+ \left| \left(\frac{\partial_+^{\alpha_l/2} u}{\partial x_{l,+}^{\alpha_l/2}}, \frac{\partial_-^{\alpha_l/2} u}{\partial x_{l,-}^{\alpha_l/2}} \right) \right| \right. \\ & \quad \left. + \sum_{l=1}^d \varepsilon_{\alpha_l}^- \left| \left(\frac{\partial_-^{\alpha_l/2} u}{\partial x_{l,-}^{\alpha_l/2}}, \frac{\partial_+^{\alpha_l/2} u}{\partial x_{l,+}^{\alpha_l/2}} \right) \right| \right\}^{1/2}, \\ \|u\|_{\alpha_l, \Omega} &= (\|u\|_{0, \Omega}^2 + |u|_{\alpha_l, \Omega}^2)^{1/2}. \end{aligned}$$

Lemma 5 [13] *The coefficients ω_k^θ enjoy the property*

$$\frac{1}{n^\theta \Gamma(1-\theta)} < \sum_{k=0}^{n-1} \omega_k^\theta = - \sum_{k=n}^\infty \omega_k^\theta \leq \frac{1}{n^\theta}, \quad (17)$$

where $n = 1, 2, 3, \dots$

In the sequel, we carry out the stability and convergent analysis for the semi-discrete scheme.

Theorem 3 *The discrete scheme (16) is unconditionally stable.*

Proof Let $\tilde{U}^n(\mathbf{x})$ be the perturbation solution of the exact solution $u^n(\mathbf{x})$ and $e^n = u^n(\mathbf{x}) - \tilde{U}^n(\mathbf{x})$. According to Eq. (16), we have the error equation

$$\begin{aligned} & \sum_{r=1}^s \frac{a_r}{\tau^{\theta_r}} e^n - \sum_{l=1}^d \varepsilon_{\alpha_l}^+ \frac{\partial_+^{\alpha_l} e^n}{\partial x_{l,+}^{\alpha_l}} - \sum_{l=1}^d \varepsilon_{\alpha_l}^- \frac{\partial_-^{\alpha_l} e^n}{\partial x_{l,-}^{\alpha_l}} \\ & = - \sum_{r=1}^s \frac{a_r}{\tau^{\theta_r}} \sum_{k=1}^{n-1} \omega_k^{\theta_r} e^{n-k} + \sum_{r=1}^s \frac{a_r}{\tau^{\theta_r}} \sum_{k=0}^{n-1} \omega_k^{\theta_r} e^0. \end{aligned}$$

By multiplying this equation by e^n and integrating it over Ω , we obtain

$$\begin{aligned} & \sum_{r=1}^s \frac{a_r}{\tau^{\theta_r}} (e^n, e^n) - \sum_{l=1}^d \varepsilon_{\alpha_l}^+ \left(\frac{\partial_+^{\alpha_l} e^n}{\partial x_{l,+}^{\alpha_l}}, e^n \right) \\ & - \sum_{l=1}^d \varepsilon_{\alpha_l}^- \left(\frac{\partial_-^{\alpha_l} e^n}{\partial x_{l,-}^{\alpha_l}}, e^n \right) = - \sum_{r=1}^s \frac{a_r}{\tau^{\theta_r}} \sum_{k=1}^{n-1} \omega_k^{\theta_r} (e^{n-k}, e^n) \\ & + \sum_{r=1}^s \frac{a_r}{\tau^{\theta_r}} \sum_{k=0}^{n-1} \omega_k^{\theta_r} (e^0, e^n). \end{aligned}$$

In view of Lemma 1, Lemma 2, we have

$$\begin{aligned} \Lambda(e^n, e^n) &= - \sum_{l=1}^d \varepsilon_{\alpha_l}^+ \left(\frac{\partial_+^{\alpha_l} e^n}{\partial x_{l,+}^{\alpha_l}}, e^n \right) - \sum_{l=1}^d \varepsilon_{\alpha_l}^- \left(\frac{\partial_-^{\alpha_l} e^n}{\partial x_{l,-}^{\alpha_l}}, e^n \right) \\ &= - \sum_{l=1}^d \varepsilon_{\alpha_l}^+ \left(\frac{\partial_+^{\alpha_l/2} e^n}{\partial x_{l,+}^{\alpha_l/2}}, \frac{\partial_-^{\alpha_l/2} e^n}{\partial x_{l,-}^{\alpha_l/2}} \right) \\ & \quad - \sum_{l=1}^d \varepsilon_{\alpha_l}^- \left(\frac{\partial_-^{\alpha_l/2} e^n}{\partial x_{l,-}^{\alpha_l/2}}, \frac{\partial_+^{\alpha_l/2} e^n}{\partial x_{l,+}^{\alpha_l/2}} \right), \end{aligned}$$

which implies $\Lambda(e^n, e^n) = |u|_{\alpha_l, \Omega} \geq 0$, and consequently

$$\begin{aligned} \sum_{r=1}^s \frac{a_r}{\tau^{\theta_r}} (e^n, e^n) &\leq - \sum_{r=1}^s \frac{a_r}{\tau^{\theta_r}} \sum_{k=1}^{n-1} \omega_k^{\theta_r} (e^{n-k}, e^n) \\ & \quad + \sum_{r=1}^s \frac{a_r}{\tau^{\theta_r}} \sum_{k=0}^{n-1} \omega_k^{\theta_r} (e^0, e^n). \end{aligned} \quad (18)$$

On the other hand, we have

$$\begin{aligned} \sum_{k=1}^{n-1} \omega_k^{\theta_r} (e^{n-k}, e^n) &\geq \sum_{k=1}^{n-1} \omega_k^{\theta_r} \frac{\|e^{n-k}\|_{0, \Omega}^2 + \|e^n\|_{0, \Omega}^2}{2}, \\ \sum_{k=0}^{n-1} \omega_k^{\theta_r} (e^0, e^n) &\leq \sum_{k=0}^{n-1} \omega_k^{\theta_r} \frac{\|e^0\|_{0, \Omega}^2 + \|e^n\|_{0, \Omega}^2}{2}. \end{aligned}$$

Substituting the above inequalities into the inequality (18) reaches to

$$\begin{aligned} \sum_{r=1}^s \frac{a_r}{\tau^{\theta_r}} \|e^n\|_{0, \Omega}^2 &\leq \sum_{r=1}^s \frac{a_r}{\tau^{\theta_r}} \left(1 + \frac{1}{2} \sum_{k=1}^{n-1} \omega_k^{\theta_r} \right) \|e^0\|_{0, \Omega}^2 \\ & \quad - \frac{1}{2} \sum_{r=1}^s \frac{a_r}{\tau^{\theta_r}} \sum_{k=1}^{n-1} \omega_k^{\theta_r} \|e^{n-k}\|_{0, \Omega}^2. \end{aligned} \quad (19)$$

Next, we use the mathematical induction to prove the unconditional stability. Noticing $\|e^1\|_{0, \Omega} \leq \|e^0\|_{0, \Omega}$ and supposing $\|e^\ell\|_{0, \Omega} \leq \|e^0\|_{0, \Omega}$, $\ell = 1, 2, \dots, n-1$, from the inequality (19), it follows that

$$\|e^n\|_{0, \Omega}^2 \leq \left(\sum_{r=1}^s \frac{a_r}{\tau^{\theta_r}} \right)^{-1} \left[\sum_{r=1}^s \frac{a_r}{\tau^{\theta_r}} \left(1 + \frac{1}{2} \sum_{k=1}^{n-1} \omega_k^{\theta_r} \right) \|e^0\|_{0, \Omega}^2 \right]$$

$$\begin{aligned}
& -\frac{1}{2} \sum_{r=1}^s \frac{a_r}{\tau^{\theta_r}} \sum_{k=1}^{n-1} \omega_k^{\theta_r} \|e^{n-k}\|_{0,\Omega}^2 \\
& \leq \left(\sum_{r=1}^s \frac{a_r}{\tau^{\theta_r}} \right)^{-1} \left[\sum_{r=1}^s \frac{a_r}{\tau^{\theta_r}} \|e^0\|_{0,\Omega}^2 \right] \\
& = \|e^0\|_{0,\Omega}^2,
\end{aligned}$$

and this completes the mathematical induction.

We have the following convergent results.

Theorem 4 *Letting $u^n(\mathbf{x})$ be the exact solution of Eqs. (1)-(2) and $U^n(\mathbf{x})$ be the approximate solution obtained by the discrete scheme (16), we have*

$$\|u^n(\mathbf{x}) - U^n(\mathbf{x})\|_{0,\Omega} \leq C\tau, \quad (20)$$

where C is a constant and $n = 1, 2, 3, \dots$

Proof Let $\vartheta^n = u^n(\mathbf{x}) - U^n(\mathbf{x})$. Subtracting Eq. (16) from Eqs. (1)-(2) and using Theorem 2, we obtain

$$\begin{aligned}
& \sum_{r=1}^s \frac{a_r}{\tau^{\theta_r}} \vartheta^n - \sum_{l=1}^d \varepsilon_{\alpha_l}^+ \frac{\partial_{+}^{\alpha_l} \vartheta^n}{\partial x_{l,+}^{\alpha_l}} \\
& - \sum_{l=1}^d \varepsilon_{\alpha_l}^- \frac{\partial_{-}^{\alpha_l} \vartheta^n}{\partial x_{l,-}^{\alpha_l}} = - \sum_{r=1}^s \frac{a_r}{\tau^{\theta_r}} \sum_{k=1}^{n-1} \omega_k^{\theta_r} \vartheta^{n-k} + R,
\end{aligned}$$

where $\vartheta^0 = 0$ and $R = \mathcal{O}(\tau)$. Do the multiplication and integration as before, we have

$$\sum_{r=1}^s \frac{a_r}{\tau^{\theta_r}} \|\vartheta^n\|_{0,\Omega}^2 \leq - \sum_{r=1}^s \frac{a_r}{\tau^{\theta_r}} \sum_{k=1}^{n-1} \omega_k^{\theta_r} (\vartheta^{n-k}, \vartheta^n) + (R, \vartheta^n). \quad (21)$$

In view of the following inequalities

$$\sum_{k=1}^{n-1} \omega_k^{\theta_r} (\vartheta^{n-k}, \vartheta^n) \geq \sum_{k=1}^{n-1} \omega_k^{\theta_r} \frac{\|\vartheta^{n-k}\|_{0,\Omega}^2 + \|\vartheta^n\|_{0,\Omega}^2}{2},$$

$$\begin{aligned}
(R, \vartheta^n) & \leq \sum_{r=1}^s \frac{a_r}{2\tau^{\theta_r}} \sum_{k=0}^{n-1} \omega_k^{\theta_r} \|\vartheta^n\|_{0,\Omega}^2 + \frac{\|R\|_{0,\Omega}^2}{2 \sum_{r=1}^s \frac{a_r}{\tau^{\theta_r}} \sum_{k=0}^{n-1} \omega_k^{\theta_r}} \\
& \leq \sum_{r=1}^s \frac{a_r}{2\tau^{\theta_r}} \sum_{k=0}^{n-1} \omega_k^{\theta_r} \|\vartheta^n\|_{0,\Omega}^2 + \frac{\|R\|_{0,\Omega}^2}{\sum_{r=1}^s \frac{2a_r}{\tau^{\theta_r} n^{\theta_r} \Gamma(1-\theta_r)}} \\
& \leq \sum_{r=1}^s \frac{a_r}{2\tau^{\theta_r}} \sum_{k=0}^{n-1} \omega_k^{\theta_r} \|\vartheta^n\|_{0,\Omega}^2 + \frac{\|R\|_{0,\Omega}^2}{\sum_{r=1}^s \frac{2a_r}{T^{\theta_r} \Gamma(1-\theta_r)}},
\end{aligned}$$

we further obtain

$$\sum_{r=1}^s \frac{a_r}{\tau^{\theta_r}} \|\vartheta^n\|_{0,\Omega}^2$$

$$\begin{aligned}
& \leq - \sum_{r=1}^s \frac{a_r}{2\tau^{\theta_r}} \sum_{k=1}^{n-1} \omega_k^{\theta_r} (\|\vartheta^{n-k}\|_{0,\Omega}^2 + \|\vartheta^n\|_{0,\Omega}^2) \\
& + \sum_{r=1}^s \frac{a_r}{2\tau^{\theta_r}} \sum_{k=0}^{n-1} \omega_k^{\theta_r} \|\vartheta^n\|_{0,\Omega}^2 + \frac{\|R\|_{0,\Omega}^2}{\sum_{r=1}^s \frac{2a_r}{T^{\theta_r} \Gamma(1-\theta_r)}} \\
& \leq - \sum_{r=1}^s \frac{a_r}{2\tau^{\theta_r}} \sum_{k=1}^{n-1} \omega_k^{\theta_r} \|\vartheta^{n-k}\|_{0,\Omega}^2 \\
& + \sum_{r=1}^s \frac{a_r}{2\tau^{\theta_r}} \|\vartheta^n\|_{0,\Omega}^2 + \frac{\|R\|_{0,\Omega}^2}{\sum_{r=1}^s \frac{2a_r}{T^{\theta_r} \Gamma(1-\theta_r)}}
\end{aligned}$$

by using Lemma 5 and substituting the above inequalities into the inequality (21). Then, there exists

$$\begin{aligned}
& \sum_{r=1}^s \frac{a_r}{\tau^{\theta_r}} \|\vartheta^n\|_{0,\Omega}^2 \\
& \leq - \sum_{r=1}^s \frac{a_r}{\tau^{\theta_r}} \sum_{k=1}^{n-1} \omega_k^{\theta_r} \|\vartheta^{n-k}\|_{0,\Omega}^2 + C_e \|R\|_{0,\Omega}^2, \quad (22)
\end{aligned}$$

$$\text{where } C_e = 1 / \sum_{r=1}^s \frac{a_r}{T^{\theta_r} \Gamma(1-\theta_r)}.$$

Let $a_m = \min\{a_1, a_2, \dots, a_s\}$, $\theta_m = \min\{\theta_1, \theta_2, \dots, \theta_s\}$, and continue to prove the following inequality

$$\sum_{r=1}^s \frac{a_r}{\tau^{\theta_r}} \|\vartheta^n\|_{0,\Omega}^2 \leq C_e \left(\sum_{k=0}^{n-1} \omega_k^{\theta_m} \right)^{-1} \|R\|_{0,\Omega}^2 \quad (23)$$

via the mathematical induction to achieve the error bound (20). If $0 < \theta_m < 1$, then for $n = 1$, we can easily check its correctness. Supposing

$$\sum_{r=1}^s \frac{a_r}{\tau^{\theta_r}} \|\vartheta^\ell\|_{0,\Omega}^2 \leq C_e \left(\sum_{k=0}^{\ell-1} \omega_k^{\theta_m} \right)^{-1} \|R\|_{0,\Omega}^2 \quad (24)$$

with $\ell = 1, 2, \dots, n-1$, for $\ell = n$, we can prove

$$\begin{aligned}
& \sum_{r=1}^s \frac{a_r}{\tau^{\theta_r}} \|\vartheta^n\|_{0,\Omega}^2 \\
& \leq - \sum_{r=1}^s \frac{a_r}{\tau^{\theta_r}} \sum_{k=1}^{n-1} \omega_k^{\theta_r} \|\vartheta^{n-k}\|_{0,\Omega}^2 + C_e \|R\|_{0,\Omega}^2 \\
& \leq - C_e \sum_{k=1}^{n-1} \omega_k^{\theta_m} \left(\sum_{k=0}^{n-k-1} \omega_k^{\theta_m} \right)^{-1} \|R\|_{0,\Omega}^2 + C_e \|R\|_{0,\Omega}^2 \\
& \leq - C_e \sum_{k=1}^{n-1} \omega_k^{\theta_m} \left(\sum_{k=0}^{n-1} \omega_k^{\theta_m} \right)^{-1} \|R\|_{0,\Omega}^2 + C_e \|R\|_{0,\Omega}^2 \\
& \leq C_e \left(1 - \sum_{k=0}^{n-1} \omega_k^{\theta_m} \right) \left(\sum_{k=0}^{n-1} \omega_k^{\theta_m} \right)^{-1} \|R\|_{0,\Omega}^2 + C_e \|r^n\|_{0,\Omega}^2 \\
& \leq C_e \left(\sum_{k=0}^{n-1} \omega_k^{\theta_m} \right)^{-1} \|R\|_{0,\Omega}^2,
\end{aligned}$$

with the aid of (22) and $-1 < \omega_k^{\theta_r} < 0$ for $k \neq 0$. Further, letting $\tau < 1$ and using Lemma 5, we have

$$\frac{sa_m}{\tau^{\theta_m}} \|\vartheta^n\|_{0,\Omega}^2 \leq \sum_{r=1}^s \frac{a_r}{\tau^{\theta_r}} \|\vartheta^n\|_{0,\Omega}^2 \leq C_e n^{\theta_m} \Gamma(1 - \theta_m) \|R\|_{0,\Omega}^2$$

After simple operations, we obtain

$$\|\vartheta^n\|_{0,\Omega}^2 \leq \frac{C_e T^{\theta_m} \Gamma(1 - \theta_m)}{sa_m} \|R\|_{0,\Omega}^2 \leq C\tau^2.$$

On the other hand, if $\theta_m = 1$, then $\theta_1 = \theta_2 = \dots = \theta_s = 1$ and the above inequality fails to evaluate the error estimate because $\Gamma(1 - \theta_m)$ is infinity when θ_m is infinitely close to 1. Therefore, other form is needed to be found. Supposing

$$\sum_{r=1}^s \frac{a_r}{\tau} \|\vartheta^\ell\|_{0,\Omega}^2 \leq C_e \ell \|R\|_{0,\Omega}^2, \quad (25)$$

with $\ell = 1, 2, \dots, n-1$, and noticing (25) is correct for $n=1$, we check by (22) that (25) holds for $\ell=n$, i.e.,

$$\begin{aligned} & \sum_{r=1}^s \frac{a_r}{\tau} \|\vartheta^n\|_{0,\Omega}^2 \\ & \leq - \sum_{r=1}^s \frac{a_r}{\tau} \sum_{k=1}^{n-1} \omega_k^{\theta_r} \|\vartheta^{n-k}\|_{0,\Omega}^2 + C_e \|R\|_{0,\Omega}^2, \\ & \leq -C_e \sum_{k=1}^{n-1} \omega_k^{\theta_m} (n-k) \|R\|_{0,\Omega}^2 + C_e \|R\|_{0,\Omega}^2 \\ & \leq C_e \left(1 - \sum_{k=0}^{n-1} \omega_k^{\theta_m} \right) (n-k) \|R\|_{0,\Omega}^2 + C_e \|R\|_{0,\Omega}^2 \\ & \leq C_e (n-1) \|R\|_{0,\Omega}^2 + C_e \|R\|_{0,\Omega}^2 \\ & = C_e n \|R\|_{0,\Omega}^2, \end{aligned}$$

which further yields

$$\|\vartheta^n\|_{0,\Omega}^2 \leq \frac{C_e T}{sa_m} \|R\|_{0,\Omega}^2 \leq C\tau^2,$$

and this finally completes the proof.

5 Spatial discretization by RBFs-based DQ method

5.1 Discretization of fractional derivatives in space

Supposing $u(\mathbf{x}) \in C^m(\Omega)$, $m \in \mathbb{Z}^+$, we have the following DQ formula [43]:

$$u_{x_l}^{(m)}(\mathbf{x}_i, t) \approx \sum_{j=0}^M w_{ij}^{m_l} u(\mathbf{x}_j, t), \quad i = 0, 1, \dots, M,$$

where $1 \leq l \leq d$, $w_{ij}^{m_l}$, $i, j = 0, 1, \dots, M$, are the weighted coefficients. Realizing its essence and a function in the linear space V_h spanned by $\{\phi_k(\mathbf{x})\}_{k=0}^M$ can be approximately expanded as a weighted sum of $\{\phi_k(\mathbf{x})\}_{k=0}^M$, i.e., $u(\mathbf{x}, t) \approx \sum_{k=0}^M \delta_k(t) \phi_k(\mathbf{x})$, $\mathbf{x} \in \Omega \subset \mathbb{R}^d$. Then for $\frac{\partial_{+}^{\alpha} u(\mathbf{x}, t)}{\partial x_{l,+}^{\alpha}}$, we therefore raise the following DQ formulas to the left-hand fractional derivatives:

$$\begin{aligned} \frac{\partial_{+}^{\alpha} u(\mathbf{x}_i, t)}{\partial x_{l,+}^{\alpha}} & \approx \sum_{k=0}^M \delta_k(t) \frac{\partial_{+}^{\alpha} \phi_k(\mathbf{x}_i)}{\partial x_{l,+}^{\alpha}} \\ & = \sum_{k=0}^M \delta_k(t) \sum_{j=0}^M w_{ij}^{\alpha_l^+} \phi_k(\mathbf{x}_j) \approx \sum_{j=0}^M w_{ij}^{\alpha_l^+} u(\mathbf{x}_j, t), \end{aligned} \quad (26)$$

in which, $w_{ij}^{\alpha_l^+}$, $i, j = 0, 1, \dots, M$, fulfill

$$\frac{\partial_{+}^{\alpha} \phi_k(\mathbf{x}_i)}{\partial x_{l,+}^{\alpha}} = \sum_{j=0}^M w_{ij}^{\alpha_l^+} \phi_k(\mathbf{x}_j), \quad i, k = 0, 1, \dots, M, \quad (27)$$

with $\{\phi_k(\mathbf{x})\}_{k=0}^M$ being the test functions. The ones for the fractional derivatives in other coordinate directions are defined analogously.

Since the interpolation matrices of Inverse Multi-quadrics, Inverse Quadratics and Gaussians invertible, eliminate the polynomial term in Eq. (7) and let $\phi_k(\mathbf{x}) = \varphi(r_k)$ in Eq. (27). As for Multi-quadrics, we employ

$$u(\mathbf{x}, t) \approx \sum_{i=0}^M \lambda_i(t) \varphi(r_i) + \mu_1(t).$$

Besides, from Eq. (8), it follows that $\lambda_0(t) = -\sum_{i=1}^M \lambda_i(t)$, which leads to

$$u(\mathbf{x}, t) \approx \sum_{i=1}^M \lambda_i(t) \{\varphi(r_i) - \varphi(r_0)\} + \mu_1(t).$$

By careful observation, we regard $\phi_0(\mathbf{x}) = 1$, $\phi_i(\mathbf{x}) = \varphi(r_i) - \varphi(r_0)$, $i = 1, 2, \dots, M$, as test functions. Referring to these discussions, we can get the weighted coefficients via a linear system of $M+1$ equations resulting from the above equations for the given $\{\mathbf{x}_i\}_{i=0}^M$.

5.2 Fully discrete RBFs-based DQ scheme

In this subsection, we develop a fully discrete DQ scheme for the multi-term TSFPDEs, which utilizes the operator \mathcal{A}_q^{θ} to handle the Caputo derivative in time and the RBFs-based DQ formulas to discretize the fractional derivatives in space. Let $\{\mathbf{x}_i\}_{i=0}^M$ be a set of nodes in

$\Omega \subset \mathbb{R}^d$. Replacing the space-fractional derivatives by RBFs-based DQ formulas in Eq. (15), we have

$$\begin{aligned} \sum_{r=1}^s a_r \mathcal{A}_q^{\theta_r} u(\mathbf{x}_i, t_n) - \sum_{l=1}^d \varepsilon_{\alpha_l}^+(\mathbf{x}_i) \sum_{j=0}^M w_{ij}^{\alpha_l^+} u(\mathbf{x}_j, t_n) \\ - \sum_{l=1}^d \varepsilon_{\alpha_l}^-(\mathbf{x}_i) \sum_{j=0}^M w_{ij}^{\alpha_l^-} u(\mathbf{x}_j, t_n) = f(\mathbf{x}_i, t_n) + \mathcal{O}(\tau^q). \end{aligned} \quad (28)$$

where $i = 0, 1, \dots, M$. Omitting $\mathcal{O}(\tau^q)$ and enforcing Eq. (28) to be exactly true at $\{\mathbf{x}_i\}_{i=0}^M$, we obtain the following fully discrete DQ scheme:

$$\begin{cases} \sum_{r=1}^s \frac{a_r \omega_0^{q, \theta_r}}{\tau^{\theta_r}} u(\mathbf{x}_i, t_n) - \sum_{l=1}^d \varepsilon_{\alpha_l}^+(\mathbf{x}_i) \sum_{j=0}^M w_{ij}^{\alpha_l^+} u(\mathbf{x}_j, t_n) \\ - \sum_{l=1}^d \varepsilon_{\alpha_l}^-(\mathbf{x}_i) \sum_{j=0}^M w_{ij}^{\alpha_l^-} u(\mathbf{x}_j, t_n) = f(\mathbf{x}_i, t_n) \\ - \sum_{r=1}^s \frac{a_r}{\tau^{\theta_r}} \sum_{k=1}^{n-1} \omega_k^{q, \theta_r} u(\mathbf{x}_i, t_{n-k}) \\ + \sum_{r=1}^s \frac{a_r}{\tau^{\theta_r}} \sum_{k=0}^{n-1} \omega_k^{q, \theta_r} u(\mathbf{x}_i, 0), \quad (\mathbf{x}_i; t_n) \in \Omega \times (0, T], \\ u(\mathbf{x}_i, 0) = u_0(\mathbf{x}_i), \quad \mathbf{x}_i \in \Omega, \\ u(\mathbf{x}_i, t_n) = g(\mathbf{x}_i, t_n), \quad (\mathbf{x}_i; t_n) \in \partial\Omega \times (0, T], \end{cases} \quad (29)$$

where $i = 0, 1, \dots, M$ and $n = 1, 2, \dots, N$.

For the ease of expression, we employ the notations $U_i^n = u(\mathbf{x}_i, t_n)$, $\varepsilon_{\alpha_l, i}^\pm = \varepsilon_{\alpha_l}^\pm(\mathbf{x}_i)$, $f_i^n = f(\mathbf{x}_i, t_n)$, $g_i^n = g(\mathbf{x}_i, t_n)$, and \mathbf{U}^n , \mathbf{F}^n , \mathbf{g}^n are the column vectors consisting of U_i^n , f_i^n and g_i^n in the ascending order of subscript i , respectively. Also, we adopt $\varepsilon_{\alpha_l}^\pm = \text{diag}(\varepsilon_{\alpha_l, 0}^\pm, \varepsilon_{\alpha_l, 1}^\pm, \dots, \varepsilon_{\alpha_l, M}^\pm)$. Reforming Eqs. (29) in a matrix-vector form finally leads to

$$\begin{cases} \sum_{r=1}^s \frac{a_r \omega_0^{q, \theta_r}}{\tau^{\theta_r}} \mathbf{U}^n - \sum_{l=1}^d \varepsilon_{\alpha_l}^+ \mathbf{W}_{\alpha_l}^+ \mathbf{U}^n - \sum_{l=1}^d \varepsilon_{\alpha_l}^- \mathbf{W}_{\alpha_l}^- \mathbf{U}^n \\ = \mathbf{F}^n - \sum_{r=1}^s \frac{a_r}{\tau^{\theta_r}} \sum_{k=1}^{n-1} \omega_k^{q, \theta_r} \mathbf{U}^{n-k} + \sum_{r=1}^s \frac{a_r}{\tau^{\theta_r}} \sum_{k=0}^{n-1} \omega_k^{q, \theta_r} \mathbf{U}^0, \\ U_i^n = g_i^n, \quad \text{for } \mathbf{x}_i \in \partial\Omega, \end{cases} \quad (30)$$

where $n = 0, 1, \dots, N$ and $\mathbf{W}_{\alpha_l}^\pm$ are the weighted coefficient matrices, given by

$$\mathbf{W}_{\alpha_l}^\pm = \begin{pmatrix} w_{00}^{\alpha_l^\pm} & w_{01}^{\alpha_l^\pm} & \dots & w_{0M}^{\alpha_l^\pm} \\ w_{10}^{\alpha_l^\pm} & w_{11}^{\alpha_l^\pm} & \dots & w_{1M}^{\alpha_l^\pm} \\ \vdots & \vdots & \ddots & \vdots \\ w_{M0}^{\alpha_l^\pm} & w_{M1}^{\alpha_l^\pm} & \dots & w_{MM}^{\alpha_l^\pm} \end{pmatrix}, \quad l = 1, 2, \dots, d.$$

In addition, before we can get the numerical solutions, another problem having to be addressed is how

to compute the fractional derivatives of RBFs and determine the corresponding integral paths. It is acknowledged that the fractional derivative of a general function like RBFs is quite difficult to compute. We will be engaged in this point. For a node $\mathbf{x}_i \in \Omega$ and the RBF $\varphi(r_i)$, letting $\xi = x_l - (x_l - X_{l,L})(1 + \zeta)/2$, one has

$$\frac{\partial_+^\alpha \varphi_k(r_i)}{\partial x_{l,+}^\alpha} = \frac{1}{\Gamma(2 - \alpha)} \left(\frac{x_l - X_{l,L}}{2} \right)^{2-\alpha} \int_{-1}^1 \left\{ (1 + \zeta)^{1-\alpha} \right. \\ \left. \cdot \frac{\partial^2 \varphi_k(r_i|_{x_l=\xi})}{\partial \xi^2} \right|_{\xi=x_l-(x_l-X_{l,L})(1+\zeta)/2} \} d\zeta,$$

where $X_{l,L} = \min \{ \eta_l : (\eta_1, \eta_2, \dots, \eta_d), \eta_i = x_i, i \neq l \}$. Then, it can be tackled by Gauss-Jacobi quadrature formula [35]. The line segment along the x_l -coordinate axis from the left-side of boundary to the node \mathbf{x}_i is called the integral path, which need to be determined before the calculation of fractional derivatives.

By solving the algebraic equations resulting from the RBFs-based DQ scheme (30), we obtain the desirable solutions for the considered problems at each time layer through an iterative procedure. From the constructive process of the scheme, we can observe that the treatment of boundary conditions is pretty simple and no special treatment is required, which is one of the advantages of our approach. Because it is not pure RBFs method based on interpolation, we do not have to compute the unknown weights in interpolation and rearrange the unknown function in RBFs interpolation form, therefore the proposed DQ method can easily be applied to the nonlinear fractional problems.

6 Illustrative examples

Let u_i^n , U_i^n be the analytical and numerical solutions at the time level n . Denoting

$$\|u - U\|_{L^2} = \left[h^* \sum_{i=0}^M (u_i^n - U_i^n)^2 \right]^{\frac{1}{2}}, \quad h^* = \frac{1}{M+1}, \\ \|u - U\|_{L^\infty} = \max_{0 \leq i \leq M} |u_i^n - U_i^n|,$$

some illustrative examples will be performed to reveal the validity and convergence of the proposed RBFs-based DQ method on different domains. We test our codes by choosing the values of the shape parameters with reference to the formula $c = \nu/(M+1)^{\sigma/4}$, where $\nu > 0$, $\sigma \in \mathbb{Z}^+$, and solve all one-dimensional problems on the nodal distribution $x_i = (1 - \cos \frac{i\pi}{M})(b-a)/2 + a$, $i = 0, 1, \dots, M$, when $\Omega = [a, b]$. We compute the con-

vergent rates by

$$\text{Cov. rate} = \begin{cases} \frac{\log_2 \left(\|u - U\|_{L^\nu} / \|u - U\|_{L^\nu}^* \right)}{\log_2(\tau_2/\tau_1)}, & \text{in time,} \\ \frac{\log_2 \left(\|u - U\|_{L^\nu} / \|u - U\|_{L^\nu}^* \right)}{\log_2(M_2/M_1)}, & \text{in space,} \end{cases}$$

where $\nu = 2, \infty, \tau_1, \tau_2, M_1, M_2$ are the temporal step-sizes and nodal parameters, $\|u - U\|_{L^\nu}, \|u - U\|_{L^\nu}^*$ are the numerical errors, which correspond to τ_1, M_1 and τ_2, M_2 , respectively. τ_1, τ_2, M_1 , and M_2 should satisfy the conditions $\tau_1 \neq \tau_2$ and $M_1 \neq M_2$. We numerically study the convergent accuracy of the proposed RBFs-based DQ method in time and space by comparing with some existing algorithms like FD and FE methods. According to the theoretical analysis, we anticipate the errors yielded by the DQ method would show a gradual decline as M increases and the convergent rate in time would strictly be q as τ decreases. Moreover, all the numerical tests are carried out by MATLAB R2014a on a personal PC with WIN 7 Pro., AMD Athlon(tm) II $\times 2$ 250 3.00 GHz Processor and 4 GB DDR3 RAM.

6.1 One-dimensional problems

Example 6.1. To test the validity of the DQ formula, we discretize ${}_0^C D_x^\alpha (x+1)^3$ on $[-1, 1]$ by Grünwald-Letnikov (GL) difference operator and DQ formula. We choose $\alpha = 1.5$ and Inverse Multiquadratics as the test functions with the free parameters $\nu = 1.3$ and $\sigma = 1$. The comparison of numerical errors and convergent rates for these two methods are shown in Table 2. It is clear from this table that the convergent rates of GL-operator are strictly 1 throughout the whole computation, while DQ formula has far better performance than GL-operator on aspects of both convergent rates and mean square errors. Thus, we come to the conclusion that our DQ formulas have been exhibited to be more efficient than GL-operator.

Example 6.2. Consider the one-dimensional multi-term TSFDE:

$$\begin{cases} \sum_{r=1}^4 a_{r0} {}_0^C D_t^{\theta_r} u(x, t) - \frac{\partial_+^\alpha u(x, t)}{\partial x_+^\alpha} = \sum_{r=1}^4 \frac{120a_r t^{5-\theta_r} x^4}{\Gamma(6-\theta_r)} \\ \quad - \frac{24t^5 x^{4-\alpha}}{\Gamma(5-\alpha)}, \quad (x, t) \in [0, 1] \times (0, T], \\ u(x, 0) = 0, \quad x \in [0, 1], \\ u(0, t) = 0, \quad u(1, t) = t^5, \quad t \in (0, T], \end{cases}$$

with $a_1 = a_2 = a_3 = a_4 = 1$, $\theta_1 = 0.3$, $\theta_2 = 0.5$, $\theta_3 = 0.7$, $\theta_4 = 0.9$ and $\alpha = 1.2$.

The analytical solution is $u(x, t) = t^5 x^4$. Using Multiquadratics and Inverse Quadratics as the test functions and choosing the corresponding free parameters by $\nu = 0.1$, $\sigma = 1$ and $\nu = 0.3$, $\sigma = 1$, respectively, the convergent results in space at $t = 0.5$ with $q = 1$, $\tau = 5.0 \times 10^{-5}$ are listed in Table 3. The comparison of numerical, analytical solutions and the resulting absolute error yielded by IQ-based DQ method at $t = 0.5$ when $M = 25$ are plotted in Fig. 1. As expected, we obviously see that the errors are quite small and the convergent rates are almost up to 4, which implies that the proposed DQ method achieves high accuracy by using a small number of nodes. The results in the figure show the good consistency between the numerical and analytical solutions, and the error reaches its peak at the nodes where the analytical solution changes dramatically. Besides, MQ-based DQ method does better than IQ-based DQ method in solving this problem, while the magnitudes of the associated convergent rates for both two methods have a completely opposite relation. Furthermore, we examine the convergent rates of MQ-based DQ method in time with different q . For this purpose, retaking $\nu = 0.15$, $\sigma = 1$, $q = 1, 2, 3, 4$, and $M = 50$, the numerical errors and corresponding convergent rates at $t = 0.5$ are all shown in Table 4. From the data of this table, we observe that the convergent rates of our method are nearly $\mathcal{O}(\tau^q)$ in time, which is basically what we anticipated in theory.

6.2 Two-dimensional problems

Example 6.3. Consider the two-dimensional single-term TSFDE:

$$\begin{cases} {}_0^C D_t^\theta u(x, y, t) + \frac{1}{2 \cos(\alpha\pi/2)} \left(\frac{\partial_+^\alpha u(x, y, t)}{\partial x_+^\alpha} + \frac{\partial_-^\alpha u(x, y, t)}{\partial x_-^\alpha} \right) \\ \quad + \frac{1}{2 \cos(\beta\pi/2)} \left(\frac{\partial_+^\beta u(x, y, t)}{\partial y_+^\beta} + \frac{\partial_-^\beta u(x, y, t)}{\partial y_-^\beta} \right) \\ \quad = f(x, y, t), \quad (x, y, t) \in \Omega \times (0, T], \\ u(x, y, 0) = x^2(1-x)^2 y^2(1-y)^2, \quad (x, y) \in \Omega, \\ u(x, y, t) = 0, \quad (x, y, t) \in \partial\Omega \times (0, T], \end{cases}$$

on the square domain with $\Omega = [0, 1] \times [0, 1]$, $\alpha = \beta = 1.6$ and the source term

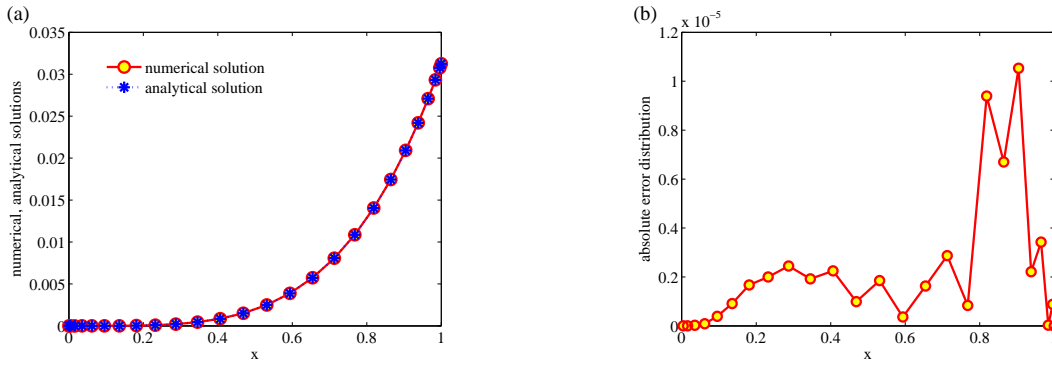
$$\begin{aligned} f(x, y, t) = & \frac{2t^{2-\theta}}{\Gamma(3-\theta)} x^2(1-x)^2 y^2(1-y)^2 \\ & + \frac{(1+t^2)y^2(1-y)^2}{\cos(\alpha\pi/2)} \left\{ \frac{x^{2-\alpha} + (1-x)^{2-\alpha}}{\Gamma(3-\alpha)} \right. \\ & \quad \left. - \frac{6(x^{3-\alpha} + (1-x)^{3-\alpha})}{\Gamma(4-\alpha)} + \frac{12(x^{4-\alpha} + (1-x)^{4-\alpha})}{\Gamma(5-\alpha)} \right\} \\ & + \frac{(1+t^2)x^2(1-x)^2}{\cos(\beta\pi/2)} \left\{ \frac{y^{2-\beta} + (1-y)^{2-\beta}}{\Gamma(3-\beta)} \right. \end{aligned}$$

Table 2 The comparison of errors for GL-operator and DQ formula when $\alpha = 1.5$.

M	GL-operator		DQ formula	
	$\ u - U\ _{L^2}$	Cov. rate	$\ u - U\ _{L^2}$	Cov. rate
10	3.1748e-01	-	5.4602e-01	-
15	2.1632e-01	0.95	8.7341e-02	4.52
20	1.6399e-01	0.96	2.3303e-02	4.59
25	1.3203e-01	0.97	6.8577e-03	5.48

Table 3 The convergent results at $t = 0.5$ with $q = 1$, $\tau = 5.0 \times 10^{-5}$ and different M for Example 6.2.

M	MQ-based DQ method		IQ-based DQ method,	
	$\ u - U\ _{L^2}$	Cov. rate	$\ u - U\ _{L^2}$	Cov. rate
10	6.7983e-05	-	1.3132e-04	-
15	1.7258e-05	3.38	3.1071e-05	3.55
20	6.5139e-06	3.39	9.2979e-06	4.19
25	2.9562e-06	3.54	3.3970e-06	4.51

**Fig. 1** The comparison of numerical, analytical solutions and the absolute error by IQ-based DQ method at $t = 0.5$.**Table 4** The convergent results at $t = 0.5$ of MQ-based DQ method with different q , τ and $M = 50$ for Example 6.2.

	τ	$\ u - U\ _{L^2}$	Cov. rate	$\ u - U\ _{L^\infty}$	Cov. rate
$q = 1$	1/10	2.4414e-03	-	5.0450e-03	-
	1/20	1.2432e-03	0.97	2.6025e-03	0.96
	1/40	6.2677e-04	0.99	1.3202e-03	0.98
	1/80	3.1463e-04	0.99	6.6470e-04	0.99
$q = 2$	1/10	8.5486e-04	-	1.7887e-03	-
	1/20	2.5813e-04	1.73	5.4164e-04	1.72
	1/40	7.1272e-05	1.86	1.4945e-04	1.86
	1/80	1.8741e-05	1.93	3.9271e-05	1.93
$q = 3$	1/10	3.2489e-04	-	6.7717e-04	-
	1/20	5.2081e-05	2.64	1.0742e-04	2.66
	1/40	7.2778e-06	2.84	1.4941e-05	2.85
	1/80	9.6000e-07	2.92	1.9623e-06	2.93
$q = 4$	1/10	1.0892e-04	-	2.2404e-04	-
	1/20	7.8556e-06	3.79	1.5722e-05	3.83
	1/40	5.2432e-07	3.91	1.0391e-06	3.92
	1/80	3.9482e-08	3.73	1.1705e-07	3.15

$$-\frac{6(y^{3-\beta} + (1-y)^{3-\beta})}{\Gamma(4-\beta)} + \frac{12(y^{4-\beta} + (1-y)^{4-\beta})}{\Gamma(5-\beta)} \quad [42] \quad ((p, q) = (1, 0) \text{ for WSGL1 and } (p, q) = (1, -1) \text{ for WSGL2, } p, q \text{ are weighted parameters}), \text{ FD method}$$

The analytical solution is $u(x, y, t) = (1+t^2)x^2(1-x)^2y^2(1-y)^2$. To show the superiority of our methods as much as possible, we compare the spatial accuracy of the weighted and shifted GL (WSGL) methods

[6], FE method based on bilinear rectangular finite elements [37] and our DQ method based on Inverse Multiquadratics in terms of $\|u - U\|_{L^2}$. Here, we note that the structured quadrilateral meshes with the mesh sizes

$h = 1/4$, $h = 1/8$, $h = 1/16$ and $h = 1/32$ are employed in the program running of the above FE method, i.e., the nodal numbers in turn are 25, 81, 289 and 1089, respectively. Taking $\theta = 0.5$, $\nu = 8$, $\sigma = q = 2$ and $\tau = 1.0 \times 10^{-3}$, the numerical errors at $t = 1$ of all the above-mentioned methods are reported in Table 5. From this table, we observe that the proposed DQ method is beyond all doubt more excellent than WSGL and FD methods in computational accuracy. Although the error magnitude of DQ method is about the same as bilinear rectangular FE method, it is certain that our method would be more flexible in implementation and have a less amount of computation than bilinear rectangular FE method because DQ methods do not require meshes generation in practical computation, nor is variational principle.

Furthermore, to get more insight into the computational efficiency of the proposed DQ method, we compare the spatial accuracy and CPU times of FE method based on linear unstructured triangular finite elements [50] and our DQ method with the same nodal numbers. Retaking $\theta = 1$, the numerical errors at $t = 1$ and the CPU time costs are all tabulated in Table 6, where the unstructured triangular meshes of the mesh sizes $h \approx 1/2$, $h \approx 1/4$, $h \approx 1/8$ and $h \approx 1/12$ are used in FE method with the nodal numbers exactly being 12, 37, 121 and 199, respectively. In Fig. 2, the used triangular meshes with $h \approx 1/8$ and $h \approx 1/12$ are displayed. The configuration of 199 nodes used in IMQ-based DQ method and its corresponding absolute error of IMQ-based DQ method at $t = 1$ are presented in Fig. 3. From these table and figures, we observe that DQ method achieves better accuracy than FE method does, and not only that, the CPU time of our DQ method is almost a third of that of FE method in the best situation, which further manifests that our method causes the overall computational work much less than FE method. On the other hand, the absolute error reaches a maximum in the center of the square domain and gradually decreases along the center towards the boundary, which is related to the shape of the analytical solution.

Example 6.4. Consider the two-dimensional multi-term TSFPDE:

$$\begin{cases} \sum_{r=1}^3 a_r {}^C D_t^{\theta_r} u(x, y, t) - \frac{x^\alpha}{2} \frac{\partial_+^\alpha u(x, y, t)}{\partial x_+^\alpha} \\ \quad - \frac{y^\beta}{2} \frac{\partial_+^\beta u(x, y, t)}{\partial y_+^\beta} = f(x, y, t), \quad (x, y; t) \in \Omega \times (0, T], \\ u(x, y, 0) = 0, \quad (x, y) \in \Omega, \\ u(x, y, t) = t^3 x^2 y^2, \quad (x, y; t) \in \partial\Omega \times (0, T], \end{cases}$$

on the triangular domain $\Omega = \{(x, y) | 0 \leq x \leq 1, 0 \leq y \leq 1 - x\}$ with $a_1 = 2$, $a_2 = 0.5$, $a_3 = 3$, $\theta_1 = 0.1$,

$\theta_2 = 0.3$, $\theta_3 = 0.5$, $\alpha = 1.5$, $\beta = 1.8$ and the source term

$$f(x, y, t) = \sum_{r=1}^3 \frac{6a_r t^{3-\theta_r} x^2 y^2}{\Gamma(4-\theta_r)} \\ - t^3 x^2 y^2 \left\{ \frac{1}{\Gamma(3-\alpha)} + \frac{1}{\Gamma(3-\beta)} \right\}.$$

The analytical solution is $u(x, y, t) = t^3 x^2 y^2$. We use Multiquadratics and Gaussian as the test functions and choose the corresponding free parameters by $\nu = 0.3$, $\sigma = 1$ and $\nu = 0.5$, $\sigma = 1$, respectively. The convergent results at $t = 0.5$ with $q = 3$ and $\tau = 1.0 \times 10^{-3}$ are reported in Table 7. In Fig. 4, we show the used configuration of 152 nodes and its corresponding absolute error of GA-based DQ method at $t = 0.5$. It is clear from the above table and figure that a good convergent property has been presented for both two DQ methods by continually decreasing the distances of these nodes either in sense of the mean-square error or maximum error. Moreover, the absolute error of GA-based DQ method is relatively large around the hypotenuse of this triangular domain and gradually decreases along the hypotenuse towards its two right-angle sides.

Example 6.5. Consider the two-dimensional multi-term TSFPDE:

$$\begin{cases} \sum_{r=1}^3 a_r {}^C D_t^{\theta_r} u(x, y, t) + \frac{1}{2 \cos(\alpha\pi/2)} \\ \quad \cdot \left(\frac{\partial_+^\alpha u(x, y, t)}{\partial x_+^\alpha} + \frac{\partial_-^\alpha u(x, y, t)}{\partial x_-^\alpha} \right) \\ \quad + \frac{1}{2 \cos(\beta\pi/2)} \left(\frac{\partial_+^\beta u(x, y, t)}{\partial y_+^\beta} + \frac{\partial_-^\beta u(x, y, t)}{\partial y_-^\beta} \right) \\ \quad = f(x, y, t), \quad (x, y; t) \in \Omega \times (0, T], \\ u(x, y, 0) = (4x^2 + y^2 - 1)^2/10, \quad (x, y) \in \Omega, \\ u(x, y, t) = 0, \quad (x, y; t) \in \partial\Omega \times (0, T], \end{cases}$$

on the elliptical domain $\Omega = \{(x, y) | 4x^2 + y^2 \leq 1\}$ with $a_1 = a_2 = a_3 = 1$, $\theta_1 = 0.6$, $\theta_2 = 0.7$, $\theta_3 = 1$, $\alpha = \beta = 1.6$ and the source term

$$f(x, y, t) = \sum_{r=1}^3 \frac{a_r t^{2-\theta_r}}{5\Gamma(3-\theta_r)} (4x^2 + y^2 - 1)^2 \\ + \frac{(1+t^2)}{20 \cos(\alpha\pi/2)} \left\{ (192x_l^2 + 16y^2 - 16) \frac{(x-x_l)^{2-\alpha}}{\Gamma(3-\alpha)} \right. \\ \left. + \frac{384x_l(x-x_l)^{3-\alpha}}{\Gamma(4-\alpha)} + \frac{384(x-x_l)^{4-\alpha}}{\Gamma(5-\alpha)} \right. \\ \left. + (192x_r^2 + 16y^2 - 16) \frac{(x_r-x)^{2-\alpha}}{\Gamma(3-\alpha)} \right\}$$

Table 5 The comparison of mean-square errors at $t = 1$ for WSGL, FD, FE and DQ methods when $q = 2$, $\theta = 0.5$ and $\alpha = \beta = 1.6$

M	WSGL1 [42]	WSGL2 [42]	FD method [6]	FE method [37]	IMQ-based DQ method
24	8.2885e-04	7.1069e-04	5.1926e-04	2.8397e-04	2.4378e-04
80	2.0070e-04	2.4232e-04	1.1762e-05	8.6729e-05	7.7419e-05
288	4.8865e-05	6.9518e-05	2.6904e-05	2.2360e-05	2.1523e-05
1088	1.1904e-05	1.8377e-05	6.2224e-06	5.1208e-06	6.5475e-06

Table 6 The comparison of errors at $t = 1$ and CPU times for FE and DQ methods when $q = 2$, $\theta = 1$ and $\alpha = \beta = 1.6$

M	FE method [50]			IMQ-based DQ method		
	$\ u - U\ _{L^2}$	$\ u - U\ _{L^\infty}$	CPU times/s	$\ u - U\ _{L^2}$	$\ u - U\ _{L^\infty}$	CPU times/s
11	1.4364e-03	1.9251e-03	8.4470	5.7675e-04	1.1361e-03	5.2219
36	3.8724e-04	4.1695e-04	34.0283	1.1968e-04	2.6712e-04	15.1634
120	1.2548e-04	1.9499e-04	138.7742	2.1899e-05	4.7802e-05	46.0256
198	7.8313e-05	1.2380e-04	240.2891	1.0404e-05	2.2870e-05	77.1730

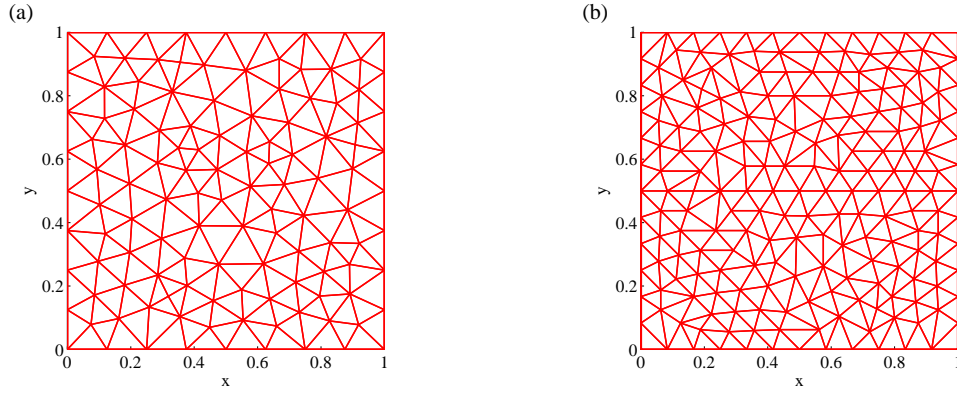


Fig. 2 The unstructured triangular meshes used by FE method with the mesh sizes $h \approx 1/8$ and $h \approx 1/12$, respectively.

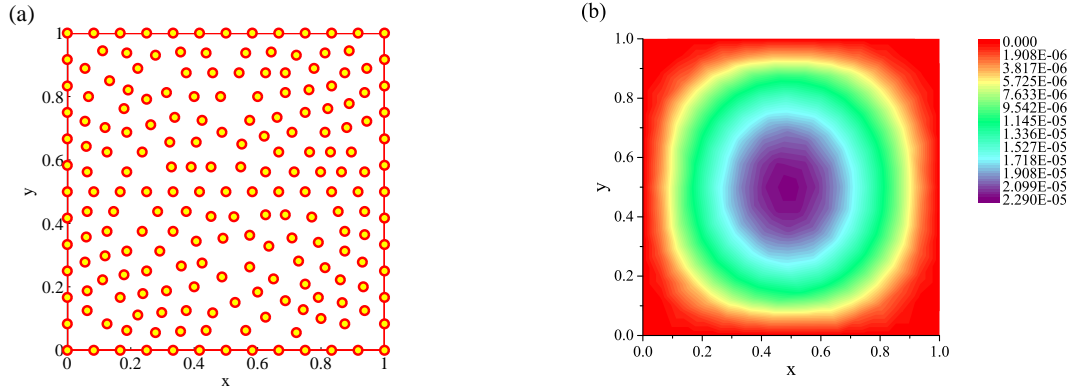


Fig. 3 The configuration of 199 nodes and its absolute error by IMQ-based DQ method at $t = 1$.

Table 7 The convergent results at $t = 0.5$ with $q = 3$, $\tau = 1.0 \times 10^{-3}$ and different M for Example 6.4

M	MQ-based DQ method		GA-based DQ method	
	$\ u - U\ _{L^2}$	$\ u - U\ _{L^\infty}$	$\ u - U\ _{L^2}$	$\ u - U\ _{L^\infty}$
55	5.7083e-05	1.8789e-04	8.2862e-05	3.0100e-04
79	4.4719e-05	1.6652e-04	5.9078e-05	2.2586e-04
114	3.8698e-05	1.5015e-04	5.2482e-05	2.0574e-04
152	2.9558e-05	1.1855e-04	3.6037e-05	1.5203e-04

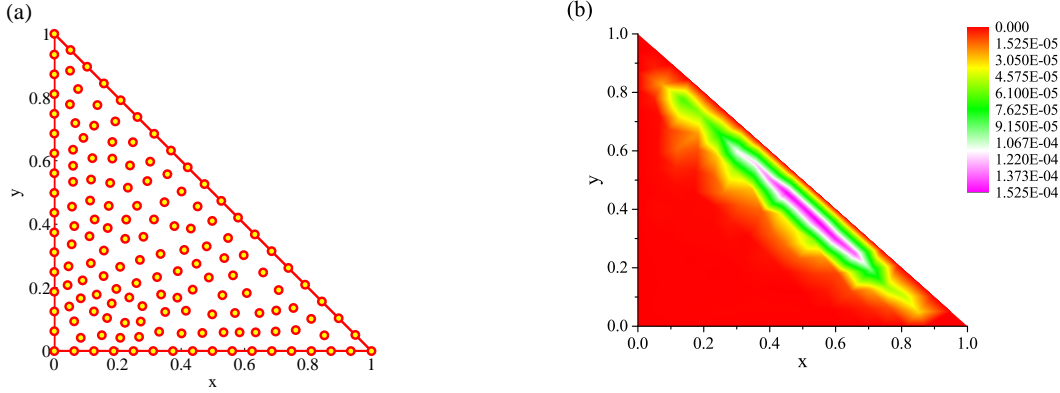


Fig. 4 The configuration of 153 nodes and its absolute error by GA-based DQ method at $t = 0.5$.

$$\begin{aligned}
 & + \frac{384x_r(x_r - x)^{3-\alpha}}{\Gamma(4-\alpha)} + \frac{384(x_r - x)^{4-\alpha}}{\Gamma(5-\alpha)} \Big\} \\
 & + \frac{(1+t^2)}{20 \cos(\beta\pi/2)} \Big\{ (192y_l^2 + 16x^2 - 16) \frac{(y - y_l)^{2-\beta}}{\Gamma(3-\beta)} \\
 & + \frac{384y_l(y - y_l)^{3-\beta}}{\Gamma(4-\beta)} + \frac{384(y - y_l)^{4-\beta}}{\Gamma(5-\beta)} \\
 & + (192y_r^2 + 16x^2 - 16) \frac{(y_r - y)^{2-\beta}}{\Gamma(3-\beta)} \\
 & + \frac{384y_r(y_r - y)^{3-\beta}}{\Gamma(4-\beta)} + \frac{384(y_r - y)^{4-\beta}}{\Gamma(5-\beta)} \Big\},
 \end{aligned}$$

with $x_l = -\sqrt{1-y^2}/2$, $x_r = \sqrt{1-y^2}/2$, $y_l = -\sqrt{1-4x^2}$ and $y_r = \sqrt{1-4x^2}$.

The analytical solution is $u(x, y, t) = \frac{1+t^2}{10}(4x^2 + y^2 - 1)^2$. We compare the spatial accuracy of FE method [27] and our DQ methods based on Inverse Quadratics and Gaussians in terms of $\|u - U\|_{L^2}$, where we choose the free parameters by $\nu = 11$, $\sigma = 2$ for Inverse Quadratics while $\nu = 4.5$, $\sigma = 2$ for Gaussians. Taking $q = 2$ and $\tau = 1.0 \times 10^{-3}$, the numerical errors at $t = 1$ of FE and DQ methods are all tabulated in Table 8. The used configurations of 113, 239 and 413 nodes and their corresponding absolute errors of IQ-based DQ method at $t = 1$ are displayed in Fig. 5. In the computation, N_e is the total number of triangles of the meshes used by the FE method. In Table 8, it can be seen that N_e is taken to be 70, 468, 1142 and 1738, respectively, then according to the proportional relationship between the numbers of nodes and triangles in a triangular mesh (the proportion of numbers of nodes to triangles is about 3:1), we know that the nodal number is bound to be much larger than N_e . Thus, we conclude that our DQ methods generate the same error magnitude as FE method with less nodes, which shows again that our DQ methods are fairly efficient and equipped with some advantages FE method does

not have. Besides, the absolute error reaches a maximum in the center of this elliptical domain and gradually decreases along the center towards its boundary, this is because the change of analytical solution is relatively rapid around the center of this domain and becomes gently in other places.

6.3 Three-dimensional problems

Example 6.6. Consider the three-dimensional multi-term TSFDE:

$$\begin{cases} \sum_{r=1}^4 a_r D_t^{\theta_r} u(x, y, z, t) - \frac{y^\gamma}{2} \frac{\partial_-^\gamma u(x, y, z, t)}{\partial z^\gamma} \\ \quad = f(x, y, z, t), \quad (x, y, z; t) \in \Omega \times (0, T], \\ u(x, y, z, 0) = 0, \quad (x, y, z) \in \Omega, \\ u(x, y, z, t) = t^3 y^{2-\gamma} (1 - x - y - z)^2, \\ \quad (x, y, z; t) \in \partial\Omega \times (0, T], \end{cases}$$

on the triangular pyramid domain $\Omega = \{(x, y, z) | 0 \leq x, y \leq 1, 0 \leq z \leq 1 - x - y\}$ with $\theta_1 = 2, \theta_2 = 1.5, \theta_3 = 2, \theta_4 = 1, a_1 = 0.2, a_2 = 0.4, a_3 = 0.7, a_4 = 0.9, \gamma = 1.8$ and the source term

$$f(x, y, z, t) = \sum_{r=1}^4 \frac{6a_r t^{3-\theta_r}}{\Gamma(4-\theta_r)} y^{2-\gamma} (1 - x - y - z)^2 - \frac{t^3 y^2 (1 - x - y - z)^{2-\gamma}}{\Gamma(3-\gamma)},$$

The analytical solution is given by $u(x, y, z, t) = t^3 y^{2-\gamma} (1 - x - y - z)^2$. We test the convergent behavior in space by using Inverse Multiquadratics and Inverse Quadratics as the test functions with the nodal numbers being 91, 119, 165 and 214. The corresponding shape parameters are selected by 0.1, 0.2, 0.9, 1 for Inverse Multiquadratics and 0.08, 0.16, 0.7, 0.8 for the latter. The convergent results at $t = 0.5$ with $q = 2$ and $\tau = 5.0 \times 10^{-4}$ are listed in Table 9. The used configuration of 119 nodes and its corresponding absolute error of IMQ-based DQ method at $t = 0.5$ are displayed in Fig. 6, respectively. It is clear from the above table and figure that the errors of these two DQ methods present a stable downward trend as we continually refine the nodes and this fact shows that our DQ methods are stable and convergent in dealing with the three-dimensional multi-term TSFPDEs. The absolute error of IMQ-based DQ method is relatively large at the nodes near the center of this triangular pyramid domain and the further the node from its center, the smaller the error looks like, which coincides with the change of analytical solution. Moreover, IMQ-based DQ method produces nearly the same accuracy as IQ-based

DQ method by using the above parameters.

Example 6.7. Consider the three-dimensional multi-term TSFDE:

$$\begin{cases} {}_0^C D_t^{\theta_1} u(x, y, z, t) + 3 {}_0^C D_t^{\theta_2} u(x, y, z, t) \\ \quad - \frac{2}{(y - 0.5 + \sqrt{0.25 - (x - 0.5)^2 - z^2})^\beta} \frac{\partial_+^\beta u(x, y, z, t)}{\partial y_+^\beta} \\ \quad = f(x, y, z, t), \quad (x, y, z; t) \in \Omega \times (0, T], \\ u(x, y, z, 0) = 0, \quad (x, y, z) \in \Omega, \\ u(x, y, z, t) = (1 + t^4) (y - 0.5 + \sqrt{0.25 - (x - 0.5)^2 - z^2})^3 z^3, \\ \quad (x, y, z; t) \in \partial\Omega \times (0, T], \end{cases}$$

on the sphere domain $\Omega = \{(x, y, z) | (x - 0.5)^2 + (y - 0.5)^2 + z^2 \leq 0.25\}$ with $\theta_1 = 0.3, \theta_2 = 0.8$ and $\beta = 1.9$. The source term is given as follows

$$f(x, y, z, t) = \left\{ \frac{12t^{4-\theta_1}}{\Gamma(5-\theta_1)} + \frac{36t^{4-\theta_2}}{\Gamma(5-\theta_2)} \right\} \cdot (y - 0.5 + \sqrt{0.25 - (x - 0.5)^2 - z^2})^3 z^3 - \frac{(1 + t^4) (y - 0.5 + \sqrt{0.25 - (x - 0.5)^2 - z^2})^3 z^3}{\Gamma(4-\beta)},$$

to enforce the analytical solution $u(x, y, z, t) = (1 + t^4) (y - 0.5 + \sqrt{0.25 - (x - 0.5)^2 - z^2})^3 z^3$.

In this test, we select $q = 4, \tau = 1.0 \times 10^{-3}$ and report the convergent results at $t = 0.5$ in Table 10, where Multiquadratics and Inverse Multiquadratics are used as the test functions and the free parameters are chosen to be $\nu = 3, \sigma = 1$ and $\nu = 3.3, \sigma = 1$, respectively. Also, we highlight the used configuration of 181 nodes and its corresponding absolute error of MQ-based DQ method at $t = 0.5$ in Fig. 7. The results observed from the table and figure illustrate that the proposed DQ methods generate the approximate solutions which are seems to be very consistent with the analytical solution and the global errors in mean-square and maximum norm sense by both two DQ methods have no big difference. Besides, the absolute error of MQ-based DQ method coincides with the change of analytical solution. Therefore, our DQ methods can be considered as a good choice in solving the three-dimensional multi-term TSFPDEs.

7 Conclusion

This investigation has considered an advanced DQ technique for the numerical solutions of the multi-term TSFPDEs on two- and three-dimensional general domains. The time discretization was basically done by high-order difference schemes and the spatial discretization was done by using a class of DQ formulas to approximate the fractional derivatives with the help of some RBFs as test functions. The unconditional stability and convergent analysis have been established for the time

Table 8 The comparison of mean-square errors at $t = 1$ for FE and DQ methods when $\theta_1 = 0.6$, $\theta_2 = 0.7$, $\theta_3 = 1$ and $\alpha = \beta = 1.6$.

N_e	FE method [27]		M	IQ-based DQ method		GA-based DQ method	
	$\ u - U\ _{L^2}$	$\ u - U\ _{L^\infty}$		$\ u - U\ _{L^2}$	$\ u - U\ _{L^\infty}$	$\ u - U\ _{L^2}$	$\ u - U\ _{L^\infty}$
70	8.6311e-03	34	7.4516e-03	1.5952e-02	6.7396e-03	1.4335e-02	
468	1.4508e-03	112	1.2389e-03	3.1296e-03	1.3671e-03	3.5605e-03	
1142	5.4919e-04	238	6.6484e-04	1.4906e-03	7.3477e-04	1.7147e-03	
1738	3.6969e-04	412	4.2034e-04	9.4854e-04	4.1947e-04	1.0285e-03	

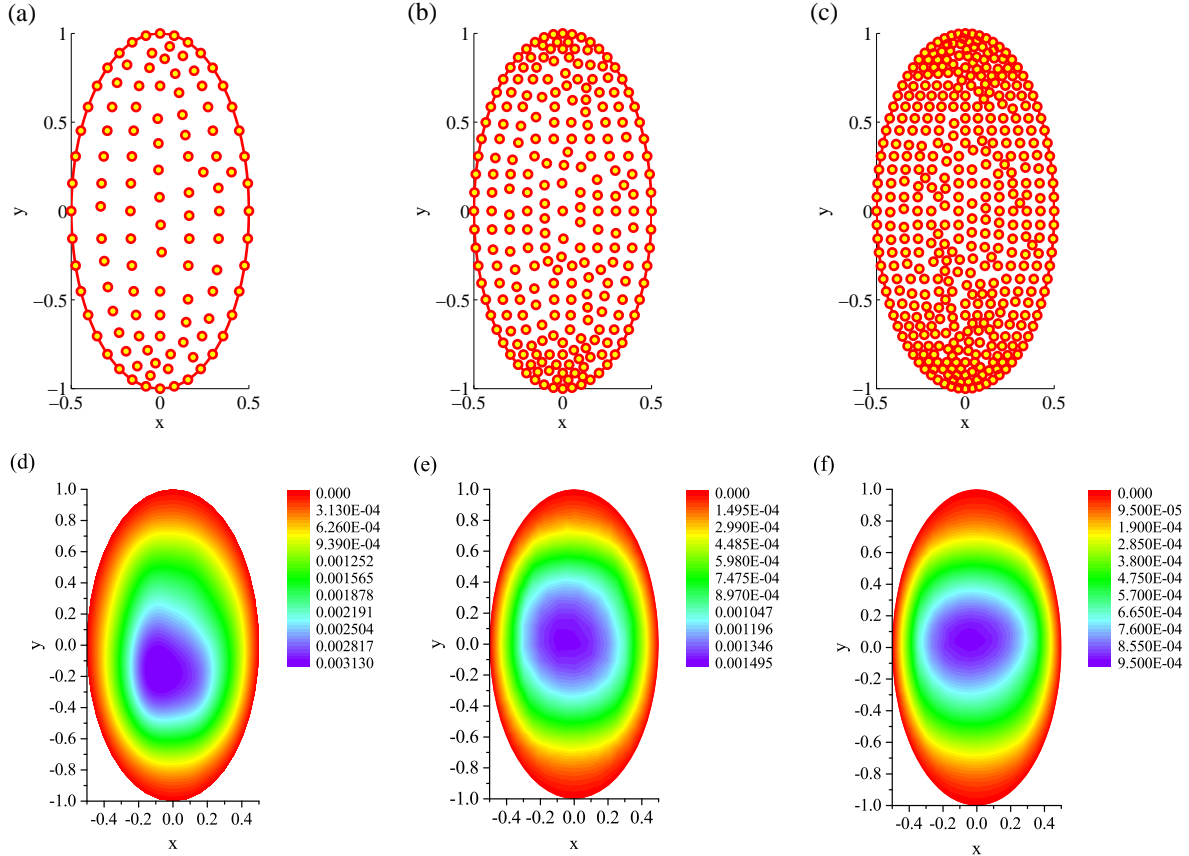


Fig. 5 The configurations of 113, 239 and 413 nodes and their absolute errors by IQ-based DQ method at $t = 1$.

Table 9 The convergent results at $t = 0.5$ with $q = 2$ and $\tau = 5.0 \times 10^{-4}$ for Example 6.6

M	IMQ-based DQ method		IQ-based DQ method	
	$\ u - U\ _{L^2}$	$\ u - U\ _{L^\infty}$	$\ u - U\ _{L^2}$	$\ u - U\ _{L^\infty}$
90	1.1210e-04	7.5967e-04	1.0397e-04	6.2086e-04
118	5.9533e-05	4.3038e-04	7.8823e-05	5.0199e-04
164	4.6240e-05	3.2299e-04	4.7980e-05	3.3329e-04
213	4.1000e-05	2.4174e-04	4.2061e-05	2.6229e-04

semi-discrete scheme. In numerical study, we applied the proposed DQ method to several typical problems. It produces very satisfactory accuracy both in time and space. The outcomes and comparisons with the true solutions or the errors yielded by the other methods like

FE method illustrate that our method is convergent with theoretical orders and effective or even more favorable in the aspect of computational accuracy.

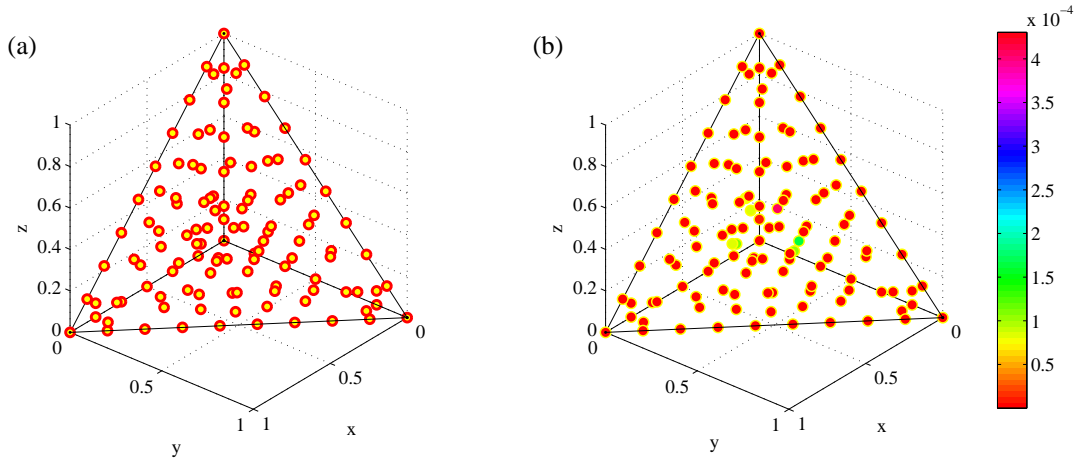


Fig. 6 The configuration of 119 nodes and its absolute error by IMQ-based DQ method at $t = 0.5$.

Table 10 The convergent results at $t = 0.5$ with $q = 4$ and $\tau = 1.0 \times 10^{-3}$ for Example 6.7

M	MQ-based DQ method		IMQ-based DQ method	
	$\ u - U\ _{L^2}$	$\ u - U\ _{L^\infty}$	$\ u - U\ _{L^2}$	$\ u - U\ _{L^\infty}$
73	1.7998e-04	8.8476e-04	1.6390e-04	8.4253e-04
101	1.2964e-04	8.0668e-04	1.2897e-04	8.1281e-04
180	5.7266e-05	4.6403e-04	5.9258e-05	4.7803e-04
336	2.1243e-05	1.3452e-04	2.2835e-05	1.4298e-04

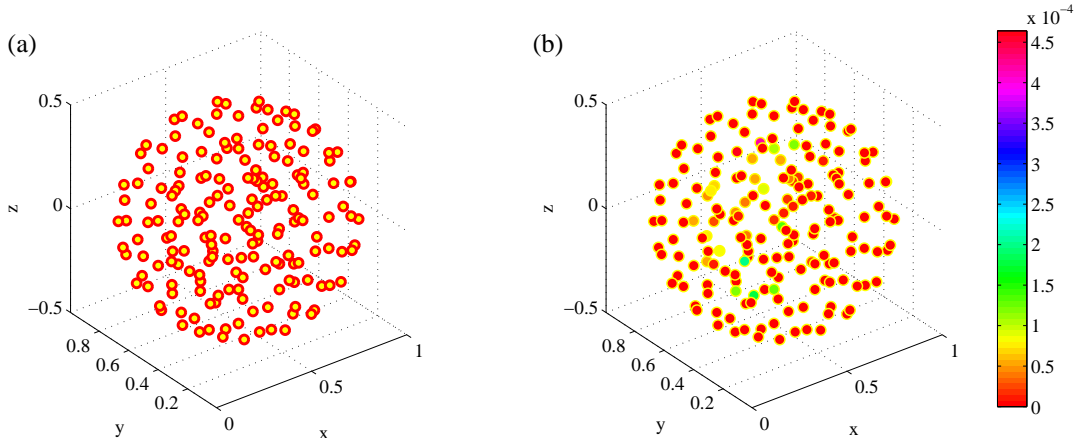


Fig. 7 The configuration of 181 nodes and its absolute error by MQ-based DQ method at $t = 0.5$.

Acknowledgements This research was supported by the Natural Science Foundation of Hunan Province of China (Nos. 2020JJ4554, 2020JJ5514), the Scientific Research Funds of Hunan Provincial Education Department (Nos. 19B509, 19C1643) and National Natural Science Foundation of China (No. 11971386).

Compliance with ethical standards

Conflict of interest The authors declare that they have no conflict of interest.

References

1. Atluri, S.N., Zhu, T.L.: A new meshless local Petrov-Galerkin (MLPG) approach in computational mechanics. *Comput. Mech.* **22**(2), 117–127 (1998)
2. Bellman, R., Casti, J.: Differential quadrature and long-term integration. *J. Math. Anal. Appl.* **34**(2), 235–238 (1971)
3. Belytschko, T., Lu, Y.Y., Gu, L.: Element-free Galerkin methods. *Int. J. Numer. Meth. Eng.* **37**(2), 229–256 (1994)
4. Bhattawy, A.H., Baleanu, D.: A spectral Legendre-Gauss-Lobatto collocation method for a space-fractional advection diffusion equations with variable coefficients. *Rep. Math. Phys.* **72**(2), 219–233 (2013)
5. Bhattawy, A.H., Zaky, M.A.: A method based on the Jacobi tau approximation for solving multi-term time-space fractional partial differential equations. *J. Comput. Phys.* **281**, 876–895 (2015)

6. Çelik, C., Duman, M.: Crank-Nicolson method for the fractional diffusion equation with the Riesz fractional derivative. *J. Comput. Phys.* **231**(4), 1743–1750 (2012)
7. Chen, M.H., Deng, W.H.: Fourth order difference approximations for space Riemann-Liouville derivatives based on weighted and shifted Lubich difference operators. *Commun. Comput. Phys.* **16**(2), 516–540 (2014)
8. Cheng, A.H.D.: Multiquadric and its shape parameter-A numerical investigation of error estimate, condition number, and round-off error by arbitrary precision computation. *Eng. Anal. Bound. Elem.* **36**(2), 220–239 (2012)
9. Cheng, J.Q., Wang, B., Du, S.Y.: A theoretical analysis of piezoelectric/composite laminate with larger-amplitude deflection effect, Part II: Hermite differential quadrature method and application. *Int. J. Solids. Struct.* **42**(24–25), 6181–6201 (2005)
10. Cheng, R.J., Sun, F.X., Wang, J.F.: Meshless analysis of two-dimensional two-sided space-fractional wave equation based on improved moving least-squares approximation. *Int. J. Comput. Math.* **95**(3), 540–560 (2018)
11. Dehghan, M., Abbaszadeh, M.: An efficient technique based on finite difference/finite element method for solution of two-dimensional space/multi-time fractional Bloch-Torrey equations. *Appl. Numer. Math.* **131**, 190–206 (2018)
12. Deng, W.H.: Finite element method for the space and time fractional Fokker-Planck equation. *SIAM J. Numer. Anal.* **47**, 204–226 (2008)
13. Deng, W.H., Chen, M.H., Barkai, E.: Numerical algorithms for the forward and backward fractional Feynman-Kac equations. *J. Sci. Comput.* **62**, 718–746 (2015)
14. Du, H., Lim, M.K., Lin, R.M.: Application of generalized differential quadrature method to structural problems. *Int. J. Numer. Meth. Eng.* **37**(11), 1881–1896 (1994)
15. Ervin, V.J., Roop, J.P.: Variational formulation for the stationary fractional advection dispersion equation. *Numer. Meth. Part. D. E.* **22**, 558–576 (2006)
16. Fan, W.P., Jiang, X.Y., Liu, F.W., Anh, V.: The unstructured mesh finite element method for the two-dimensional multi-term time-space fractional diffusion-wave equation on an irregular convex domain. *J. Sci. Comput.* **77**(1), 27–52 (2018)
17. Fedoseyev, A.I., Friedman, M.J., Kansa, E.J.: Improved multiquadric method for elliptic partial differential equations via PDE collocation on the boundary. *Comput. Math. Appl.* **43**(3–5), 439–455 (2002)
18. Fu, H.F., Sun, Y.N., Wang, H., Zheng, X.C.: Stability and convergence of a Crank-Nicolson finite volume method for space fractional diffusion equations. *Appl. Numer. Math.* **139**, 38–51 (2019)
19. Han, W.M., Meng, X.P.: Error analysis of the reproducing kernel particle method. *Comput. Method. Appl. M.* **190**(46–47), 6157–6181 (2001)
20. Hosseini, S.M., Ghaffari, R.: Polynomial and nonpolynomial spline methods for fractional sub-diffusion equations. *Appl. Math. Model.* **38**(14), 3554–3566 (2014)
21. Huang, C.B., Yu, X.J., Wang, C., Li, Z.Z., An, N.: A numerical method based on fully discrete direct discontinuous Galerkin method for the time fractional diffusion equation. *Appl. Math. Comput.* **264**, 483–492 (2015)
22. Jia, J.H., Wang, H.: Fast finite difference methods for space-fractional diffusion equations with fractional derivative boundary conditions. *J. Comput. Phys.* **293**, 359–369 (2015)
23. Jiang, Y.J., Ma, J.T.: High-order finite element methods for time-fractional partial differential equations. *J. Comput. Appl. Math.* **235**(11), 3285–3290 (2011)
24. Kansa, E.J.: Multiquadratics-A scattered data approximation scheme with applications to computational fluid-dynamics-II solutions to parabolic, hyperbolic and elliptic partial differential equations. *Comput. Math. Appl.* **19**(8–9), 147–161 (1990)
25. Kilbas, A.A.A., Srivastava, H.M., Trujillo, J.J.: *Theory and Applications of Fractional Differential Equations*. Elsevier B. V., Amsterdam (2006)
26. Lin, Y.M., Xu, C.J.: Finite difference/spectral approximations for the time-fractional diffusion equation. *J. Comput. Phys.* **225**(2), 1533–1552 (2007)
27. Liu, F.W., Feng, L.B., Anh, V., Li, J.: Unstructured-mesh Galerkin finite element method for the two-dimensional multi-term time-space fractional Bloch-Torrey equations on irregular convex domains. *Comput. Math. Appl.* **78**(5), 1637–1650 (2019)
28. Liu, F.W., Zhuang, P.H., Turner, I., Anh, V., Burrage, K.: A semi-alternating direction method for a 2-D fractional FitzHugh-Nagumo monodomain model on an approximate irregular domain. *J. Comput. Phys.* **293**, 252–263 (2015)
29. Liu, G.R., Gu, Y.T.: A point interpolation method for two-dimensional solids. *Int. J. Numer. Meth. Eng.* **50**(4), 937–951 (2001)
30. Liu, J.M., Li, X.K., Hu, X.L.: A RBF-based differential quadrature method for solving two-dimensional variable-order time fractional advection-diffusion equation. *J. Comput. Phys.* **384**, 222–238 (2019)
31. Liu, Q., Liu, F.W., Gu, Y.T., Zhuang, P.H., Chen, J., Turner, I.: A meshless method based on Point Interpolation Method (PIM) for the space fractional diffusion equation. *Appl. Math. Comput.* **256**, 930–938 (2015)
32. Meerschaert, M.M., Tadjeran, C.: Finite difference approximations for fractional advection-dispersion flow equations. *J. Comput. Appl. Math.* **172**(1), 65–77 (2004)
33. Murio, D.A.: Implicit finite difference approximation for time fractional diffusion equations. *Comput. Math. Appl.* **56**(4), 1138–1145 (2008)
34. Nayroles, B., Touzot, G., Villon, P.: Generalizing the finite element method: diffuse approximation and diffuse elements. *Comput. Mech.* **10**(5), 307–318 (1992)
35. Pang, G.F., Chen, W., Sze, K.Y.: Gauss-Jacobi-type quadrature rules for fractional directional integrals. *Comput. Math. Appl.* **66**(5), 597–607 (2013)
36. Pang, G.F., Chen, W., Sze, K.Y.: Differential quadrature and cubature methods for steady-state space-fractional advection-diffusion equations. *Comput. Model. Eng. Sci.* **97**, 299–322 (2014)
37. Qin, S.L., Liu, F.W., Turner, I.: A 2D multi-term time and space fractional Bloch-Torrey model based on bilinear rectangular finite elements. *Commun. Nonlinear Sci.* **56**, 270–286 (2018)
38. Qiu, L.L., Deng, W.H., Hesthaven, J.S.: Nodal discontinuous Galerkin methods for fractional diffusion equations on 2D domain with triangular meshes. *J. Comput. Phys.* **298**, 678–694 (2015)
39. Quan, J.R., Chang, C.T.: New insights in solving distributed system equations by the quadrature method-I. Analysis. *Comput. Chem. Eng.* **13**(7), 779–788 (1989)
40. Ren, J.C., Sun, Z.Z., Zhao, X.: Compact difference scheme for the fractional sub-diffusion equation with Neumann boundary conditions. *J. Comput. Phys.* **232**(1), 456–467 (2013)
41. Simmons, A., Yang, Q.Q., Moroney, T.: A finite volume method for two-sided fractional diffusion equations on non-uniform meshes. *J. Comput. Phys.* **335**, 747–759 (2017)

42. Tian, W.Y., Zhou, H., Deng, W.H.: A class of second order difference approximations for solving space fractional diffusion equations. *Math. Comput.* **84**(294), 1703–1727 (2015)
43. Wu, Y.L., Shu, C.: Development of RBF-DQ method for derivative approximation and its application to simulate natural convection in concentric annuli. *Comput. Mech.* **29**(6), 477–485 (2002)
44. Yang, Z.Z., Yuan, Z.B., Nie, Y.F., Wang, J.G., Zhu, X.G., Liu, F.W.: Finite element method for nonlinear Riesz space fractional diffusion equations on irregular domains. *J. Comput. Phys.* **330**, 863–883 (2017)
45. Yuan, Z.B., Nie, Y.F., Liu, F., Turner, I., Zhang, G.Y., Gu, Y.T.: An advanced numerical modeling for Riesz space fractional advection-dispersion equations by a meshfree approach. *Appl. Math. Model.* **40**(17-18), 7816–7829 (2016)
46. Yuste, S.B.: Weighted average finite difference methods for fractional diffusion equations. *J. Comput. Phys.* **216**(1), 264–274 (2006)
47. Zeng, F.H., Liu, F.W., Li, C.P., Burrage, K., Turner, I., Anh, V.: A Crank-Nicolson ADI spectral method for a two-dimensional Riesz space fractional nonlinear reaction-diffusion equation. *SIAM J. Numer. Anal.* **52**(6), 2599–2622 (2014)
48. Zhang, H., Liu, F.W., Anh, V.: Galerkin finite element approximations of symmetric space fractional partial differential equations. *Appl. Math. Comput.* **217**, 2534–2545 (2010)
49. Zhang, J.Y., Yan, G.W.: Lattice Boltzmann method for the fractional sub-diffusion equation. *Int. J. Numer. Meth. Fl.* **80**(8), 490–507 (2016)
50. Zhu, X.G., Nie, Y.F., Wang, J.G., Yuan, Z.B.: A numerical approach for the Riesz space-fractional Fisher's equation in two-dimensions. *Int. J. Comput. Math.* **94**(2), 296–315 (2017)
51. Zhu, X.G., Yuan, Z.B., Liu, F., Nie, Y.F.: Differential quadrature method for space-fractional diffusion equations on 2D irregular domains. *Numer. Algor.* **79**, 853–877 (2018)